SFTSV Infection Induces BAK/BAX-Dependent Mitochondrial DNA Release to Trigger NLRP3 Inflammasome Activation

Shufen Li, Hao Li, Yu-Lan Zhang, Qi-Lin Xin, Zhen-Qiong Guan, Xi Chen, Xiao-Ai Zhang, Xiao-Kun Li, Geng-Fu Xiao, Pierre-Yves Lozach, et al.

Article

Cell Reports

SFTSV Infection Induces BAK/BAX-Dependent Mitochondrial DNA Release to Trigger NLRP3 Inflammasome Activation

Graphical Abstract

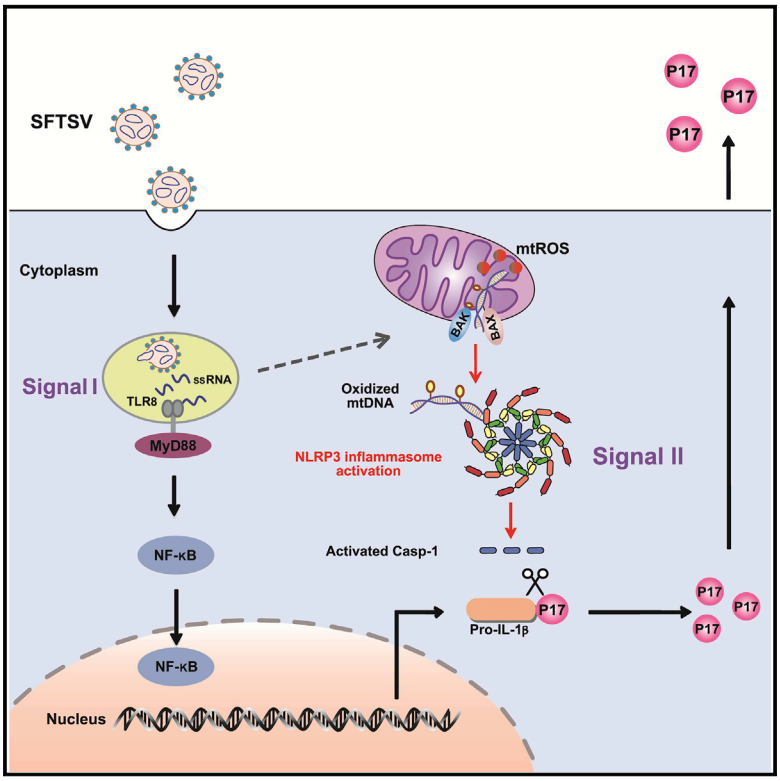

Highlights

- SFTSV induces mitochondrial damage triggering excessive inflammatory responses via NLRP3
- SFTSV induces BAK/BAX activation leading to cytosolic release of oxidized mtDNA
- The cytosolic oxidized mtDNA binds and activates NLRP3 inflammasome
- BAK expression level correlates with SFTS disease progression and fatal outcome

Authors

Shufen Li, Hao Li, Yu-Lan Zhang, ..., Wei Liu, Lei-Ke Zhang, Ke Peng

Correspondence

liuwei@bmi.ac.cn (W.L.), zhangleike@wh.iov.cn (L.-K.Z.), pengke@wh.iov.cn (K.P.)

In Brief

Li et al. reveal that mitochondrial dysfunction induced by SFTSV infection triggers excessive inflammatory responses associated with SFTS disease progression and fatal outcome. Mechanistically, SFTSV infection induces BAK/BAX activation resulting in mtDNA oxidization and cytosolic release. The cytosolic oxidized mtDNA binds to and triggers NLRP3 inflammasome activation.

Li et al., 2020, Cell Reports *30*, 4370–4385
March 31, 2020
https://doi.org/10.1016/j.celrep.2020.02.105

CellPress

OPEN ACCESS
CellPress

Cell Reports
Article

SFTSV Infection Induces BAK/BAX-Dependent Mitochondrial DNA Release to Trigger NLRP3 Inflammasome Activation

Shufen Li,[1,8] Hao Li,[2,8] Yu-Lan Zhang,[1] Qi-Lin Xin,[1] Zhen-Qiong Guan,[1,3] Xi Chen,[4] Xiao-Ai Zhang,[2] Xiao-Kun Li,[2] Geng-Fu Xiao,[1] Pierre-Yves Lozach,[5,6] Jun Cui,[7] Wei Liu,[2,*] Lei-Ke Zhang,[1,3,*] and Ke Peng[1,3,9,*]

[1]State Key Laboratory of Virology, Wuhan Institute of Virology, Center for Biosafety Mega-Science, Chinese Academy of Sciences, Wuhan, Hubei 430071, P. R. China

[2]State Key Laboratory of Pathogen and Biosecurity, Beijing Institute of Microbiology and Epidemiology, Beijing Key Laboratory of Vector Borne and Natural Focus Infectious Diseases, Beijing 100071, P. R. China

[3]University of the Chinese Academy of Sciences, Beijing 100049, P. R. China

[4]Department of Thoracic and Vascular Surgery, Wuhan No. 1 Hospital, Tongji Medical College, Huazhong University of Science and Technology, Wuhan 430022, P. R. China

[5]Department of Infectious Diseases, Virology, University Hospital Heidelberg, Heidelberg, Germany

[6]IVPC UMR754, INRA, University of Lyon, EPHE, 50 Av. Tony Garnier, 69007 Lyon, France

[7]MOE Key Laboratory of Gene Function and Regulation, State Key Lab of Biocontrol, School of Life Sciences, Sun Yat-sen University, Guangzhou 510006, P. R. China

[8]These authors contributed equally

[9]Lead Contact

*Correspondence: liuwei@bmi.ac.cn (W.L.), zhangleike@wh.iov.cn (L.-K.Z.), pengke@wh.iov.cn (K.P.)

https://doi.org/10.1016/j.celrep.2020.02.105

SUMMARY

Severe fever with thrombocytopenia syndrome (SFTS) virus (SFTSV) is an emerging tick-borne virus that carries a high fatality rate of 12%–50%. In-depth understanding of the SFTSV-induced pathogenesis mechanism is critical for developing effective anti-SFTS therapeutics. Here, we report transcriptomic analysis of blood samples from SFTS patients. We observe a strong correlation between inflammatory responses and disease progression and fatal outcome. Quantitative proteomic analysis of SFTSV infection confirms the induction of inflammation and further reveals virus-induced mitochondrial dysfunction. Mechanistically, SFTSV infection triggers BCL2 antagonist/killer 1 (BAK) upregulation and BAK/BCL2-associated X (BAX) activation, leading to mitochondrial DNA (mtDNA) oxidization and subsequent cytosolic release. The cytosolic mtDNA binds and triggers NLRP3 inflammasome activation. Notably, the BAK expression level correlates with SFTS disease progression and fatal outcome. These findings provide insights into the clinical features and molecular underpinnings of severe SFTS, which may aid in patient care and therapeutic design, and may also be conserved during infection by other highly pathogenic viruses.

INTRODUCTION

Tick-borne infectious diseases are a growing threat to public health on a global level (Paules et al., 2018). Severe fever with thrombocytopenia syndrome (SFTS) is an emerging tick-borne infectious disease caused by the banyangvirus (SFTS virus [SFTSV]) (Yu et al., 2011). SFTSV is a negative stranded RNA virus with segmented genomes and belongs to the family *Phenuiviridae* of the order Bunyavirales. The viral disease can cause severe clinical symptoms, including hemorrhagic fever, encephalitis, and multiple organ failure, with a fatality rate of 12%–50% (Kim et al., 2013; Li et al., 2018; Takahashi et al., 2014; Yu et al., 2011). The virus was first isolated in China in 2010 and then found spreading in South Korea and Japan and very recently in Vietnam (Kim et al., 2013; Li et al., 2018; Takahashi et al., 2014; Tran et al., 2019; Yu et al., 2011). The main reservoir and vector of SFTSV is *Haemaphysalis longicornis* tick, which has established a wide geographic distribution in the Australasian and Western Pacific Regions (Luo et al., 2015; Zhuang et al., 2018). Recently, this tick species was reported to be spreading in seven states and a suburb of New York City in the United States (Rainey et al., 2018), raising the possibility of potential SFTSV transmission in North America. Understanding the pathogenesis mechanism of SFTS is critical for developing effective anti-SFTS therapeutic strategies.

Inflammatory response is a key component of innate immunity and can pose an anti-viral effect against certain viruses (Chen and Ichinohe, 2015). On the other hand, excessive inflammation responses triggered by virus infection can result in severe immunopathology and fatal infection outcome (Culshaw et al., 2017; Shin et al., 2016). Maturation and secretion of the cytokine interleukin-1 beta (IL-1β) elicits a strong pro-inflammatory response and is mediated by a cytoplasmic multi-protein complex named as inflammasome (Gross et al., 2011). Inflammasomes are composed of a pattern recognition receptor (PRR) as the sensor of stimuli, an adaptor protein, in many cases, the apoptosis-associated speck-like protein containing a caspase-recruitment domain (ASC), and the cysteine protease

caspase-1 (He et al., 2016). Depending on the PRR, the inflammasomes are named as nucleotide-binding and oligomerization domain (NOD)-like receptors (NLRs; NLRP1, NLRP3, NLRC4), Pyrin, and absent in melanoma 2 (AIM2) inflammasomes (Lamkanfi and Dixit, 2014; Man and Kanneganti, 2015; Place and Kanneganti, 2018), of which NLRP3 inflammasome activation is reported to be associated with infection by a number of viruses (Chen and Ichinohe, 2015). A panel of different stimuli have been reported to activate NLRP3 inflammasome, including K^+ efflux, Ca^{2+} influx, mitochondrial reactive oxygen species (mtROS), etc. (He et al., 2016). However, none of these stimuli directly interact with NLRP3, and the mechanism of NLRP3 activation still remains elusive (Latz et al., 2013).

Mitochondria are ubiquitous eukaryotic organelles that function in multiple cellular processes (Shadel and Horvath, 2015). Recently, mitochondrion is proposed to play a key role in orchestrating innate immunity regulation mediating multiple immune signaling complexes assembly and/or directly triggering innate immune responses through mitochondrial constituents (Dhir et al., 2018; Mills et al., 2017; Zhong et al., 2018). The mitochondrial DNA (mtDNA) has several characteristics, such as its relative hypomethylation, unique structural features, and heightened susceptibility to oxidative damage, that make it a potent endogenous damage-associated molecular pattern and can activate innate sensors to trigger type I interferon (IFN) responses (West and Shadel, 2017). mtDNA is also being increasingly recognized as an agonist of the inflammasome and can potently trigger NLRP3 inflammatory responses (Shimada et al., 2012; West and Shadel, 2017; Zhou et al., 2011). Recently, mtDNA released into the cytosol was proposed to be the "ultimate" trigger of NLRP3 inflammasome under several "priming" and "activation" conditions (Shimada et al., 2012). Whether virus infection employs a similar mechanism to trigger NLRP3 activation has not been reported before.

In this study, in order to investigate the pathogenesis mechanism of SFTSV infection, we performed transcriptomic analysis of blood samples isolated from SFTS patients and quantitative proteomic analysis of SFTSV-infected cells. The integrated omics analysis showed that inflammatory responses displayed a strong correlation with disease progression and fatal outcome, and further revealed that SFTSV-induced mitochondrial dysfunction may be associated with inflammation induction. Further mechanistic investigation revealed that SFTSV infection induced mtDNA oxidation and release into the cytosol. The cytosolic mtDNA binds and activates the NLRP3 inflammasome, resulting in disease-associated inflammation responses. These findings revealed the mechanism of SFTSV-induced mtDNA-triggered NLRP3 inflammasome activation and may help development of anti-SFTS therapeutic strategies.

RESULTS

Integrated Transcriptomic and Proteomic Analyses Revealed Disease-Associated Inflammation Responses during SFTSV Infection

To investigate the pathogenesis mechanisms of SFTSV infection, we performed transcriptomic analysis with blood samples collected from SFTS patients. Patients were divided into three groups based on their clinical status: "Recover," SFTS patients during convalescence who have recovered from acute virus infection (n = 19); "Acute. Recover," SFTS patients during acute virus infection and who eventually recovered from the disease (n = 22); and "Acute. Deceased," SFTS patients during acute virus infection and who eventually died of SFTSV infection (n = 17). The group of healthy controls is composed of donors who have not experienced SFTSV infection (n = 23) (Figure S1A). In total, 81 peripheral blood samples from 40 SFTS patients and 23 healthy donors were collected, transcriptomic analysis was performed with these blood samples (Figure S1B), and differentially regulated genes relative to healthy control were summarized (Figures S1C and S1D). t-Distributed stochastic neighbor embedding (t-SNE) (van der Maaten and Hinton, 2008) analysis showed that the targeted transcriptomic profiles distinguished patients undergoing acute SFTSV infection from SFTS patients who have recovered from the acute infection and healthy controls (Figure 1A). The groups of "Acute. Recover" and "Acute. Deceased" are also separable but are relatively clustered because both groups were analyzed during the stage of acute infection. Gene ontology (GO) analysis showed that the most strongly regulated biological groups are related to "inflammatory response," "innate immune response," "complement activation," "receptor-mediated endocytosis," and "cell division" (Figure 1B). Among these biological groups, the groups of "inflammatory response" and "innate immune response" are more differently regulated when comparing the recover and the two acute infection patient groups (Figure 1C), indicating that these two groups are more strongly regulated during acute SFTSV infection. To identify factors contributing to SFTS fatal infection outcome, we analyzed the differentially regulated genes between these two acute infection patient groups, and the inflammation-related genes are the most differently regulated between these two patient groups (Figure 1D). These results indicated a potential role of virus-induced inflammatory response in SFTS fatality.

To corroborate the transcriptomic analysis and investigate the molecular mechanism of SFTSV-induced inflammation, we performed quantitative proteomic analysis of SFTSV infection in THP-1 cell, which is an inflammatory cell model that is widely used to study virus-induced inflammation (Negash et al., 2013; Wang et al., 2018). Replication kinetics analysis showed that SFTSV can productively infect THP-1 cells, and virus replication peaked at 48 h postinfection (p.i.) (Figure S2A). THP-1 cells were then infected with SFTSV at an MOI of 1 or were mock infected, and at 24, 48, and 72 h p.i., total proteins were extracted and quantified with iTRAQ-based quantitative proteomic analysis (Figure S2B). t-SNE analysis showed clear separation of samples collected at these three time points (Figure 1E). In total, 4,928 host proteins were identified, among which 147, 756, and 493 proteins were identified as being differentially regulated at 24, 48, and 72 h p.i., respectively ($p < 0.05$) (Figure S2C). Regulation of protein abundance indicated by the mass spectrometry (MS)-based quantification was verified by western blot analysis of selected candidates (Figure S2D, upper panels: upregulation; lower panels: downregulation). GO analysis showed that, consistent with the transcriptomic analysis, the "inflammatory

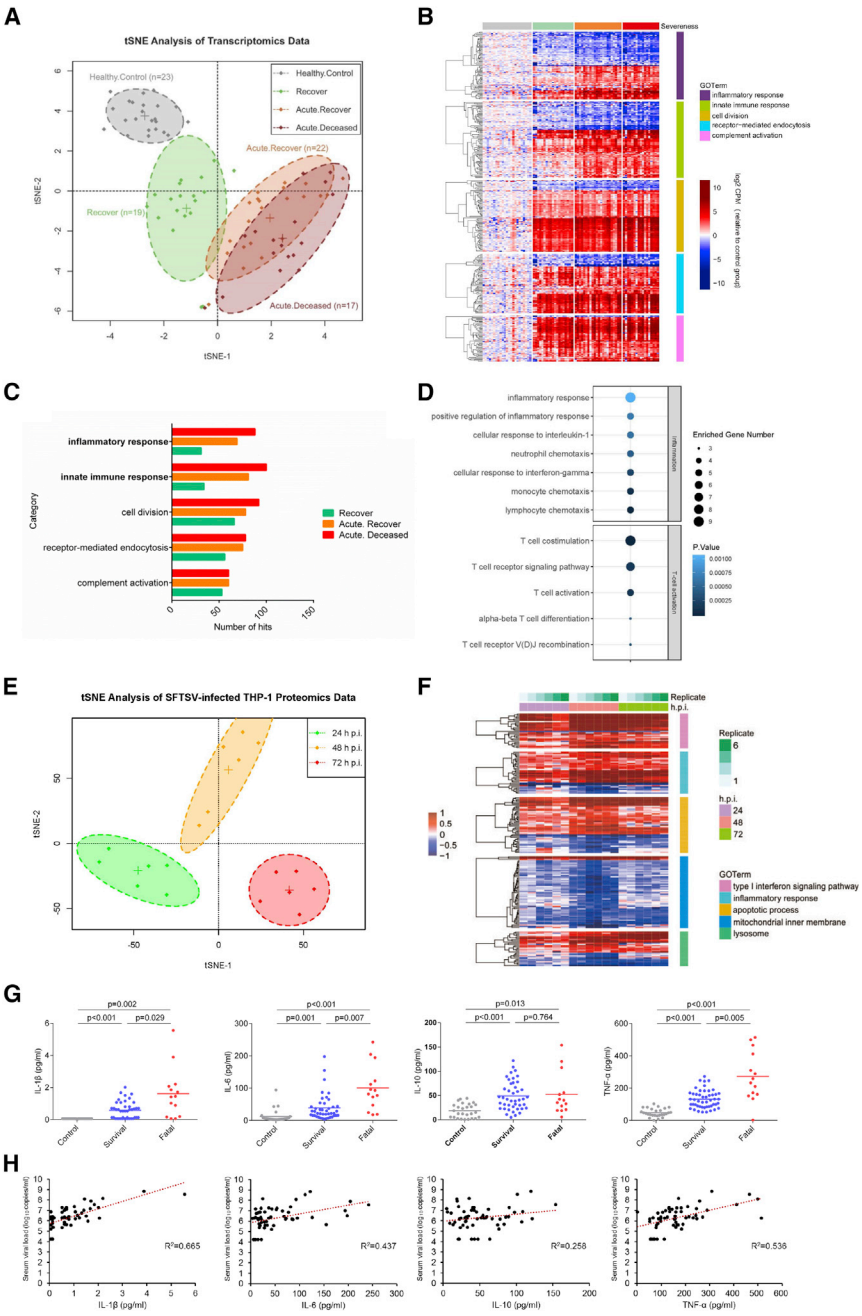

Figure 1. Transcriptomic and Proteomic Analyses Reveal the Activation of Inflammation by SFTSV

(A–D) Transcriptomic analysis of whole blood isolated from four groups of patients: Healthy control, Recover, Acute. Recover, and Acute. Deceased.

(A) t-Distributed stochastic neighbor embedding (t-SNE) plot of transcriptomic data on four groups.

(B) Heatmap profiling expression of SFTSV-regulated genes in the top 5 enriched terms presented by gene ontology (GO) analysis.

(C) Number of differentially regulated mRNAs (hits) in the top 5 enriched terms in (B).

(D) GO analysis of differentially regulated genes between Acute. Recover and Acute. Deceased.

(E) t-SNE plot of proteomic data on three time points.

(F) Heatmap profiling of SFTSV-regulated proteins expression in the top 5 enriched terms presented by GO analysis.

(G) Cytokine levels in the sera of patients and healthy controls. Comparison of mean values was analyzed by Student's t test. *$p < 0.05$; **$p < 0.01$.

(H) The correlation between viral load and cytokine levels in the sera of general SFTS patients. R^2 was evaluated by Pearson's analysis.

See also Figures S1 and S2.

response'' is among the most regulated protein groups (Figure 1F). The other regulated groups are ''type I interferon signaling pathway,'' ''apoptotic process,'' ''mitochondrial inner membrane,'' and ''lysosome'' (Figure 1F).

Because both transcriptomic and proteomic analyses revealed potent inflammatory responses triggered by SFTSV infection, we next analyzed the potential correlation between SFTSV-induced inflammatory responses and disease progression. To this aim, serum samples were collected from healthy donors and SFTS patients, and the levels of inflammatory cytokines IL-1β, IL-6, IL-10, and tumor necrosis factor alpha (TNF-α) were quantitated. The serum samples from SFTS patients were collected during hospital admission, and patients were categorized into the group of ''survival,'' representing those who recovered from the disease in the end, and ''fatal,'' representing those who died of severe infection. The levels of these four cytokines were significantly higher in survival SFTS patients than in the healthy controls (Figure 1G). Furthermore, the levels of IL-1β, IL-6, and TNF-α were significantly higher in SFTS patients who died of severe infection than those patients who recovered from the disease. The viral load in the patient serum was also determined, and the level of IL-1β and IL-6 significantly correlated with the viral load (Figure 1H). These results together supported a correlation between virus-triggered inflammatory responses and disease progression and fatal outcome in SFTS patients.

SFTSV Infection Induces IL-1β Maturation and Release in Multiple Cell Models

To investigate the molecular mechanism of SFTSV-induced inflammation activation, we analyzed whether SFTSV infection can trigger inflammatory responses in several inflammatory cell models. First, human peripheral blood mononuclear cells (PBMCs) were prepared from healthy donors and infected with SFTSV. SFTSV infection of PBMCs led to upregulation of

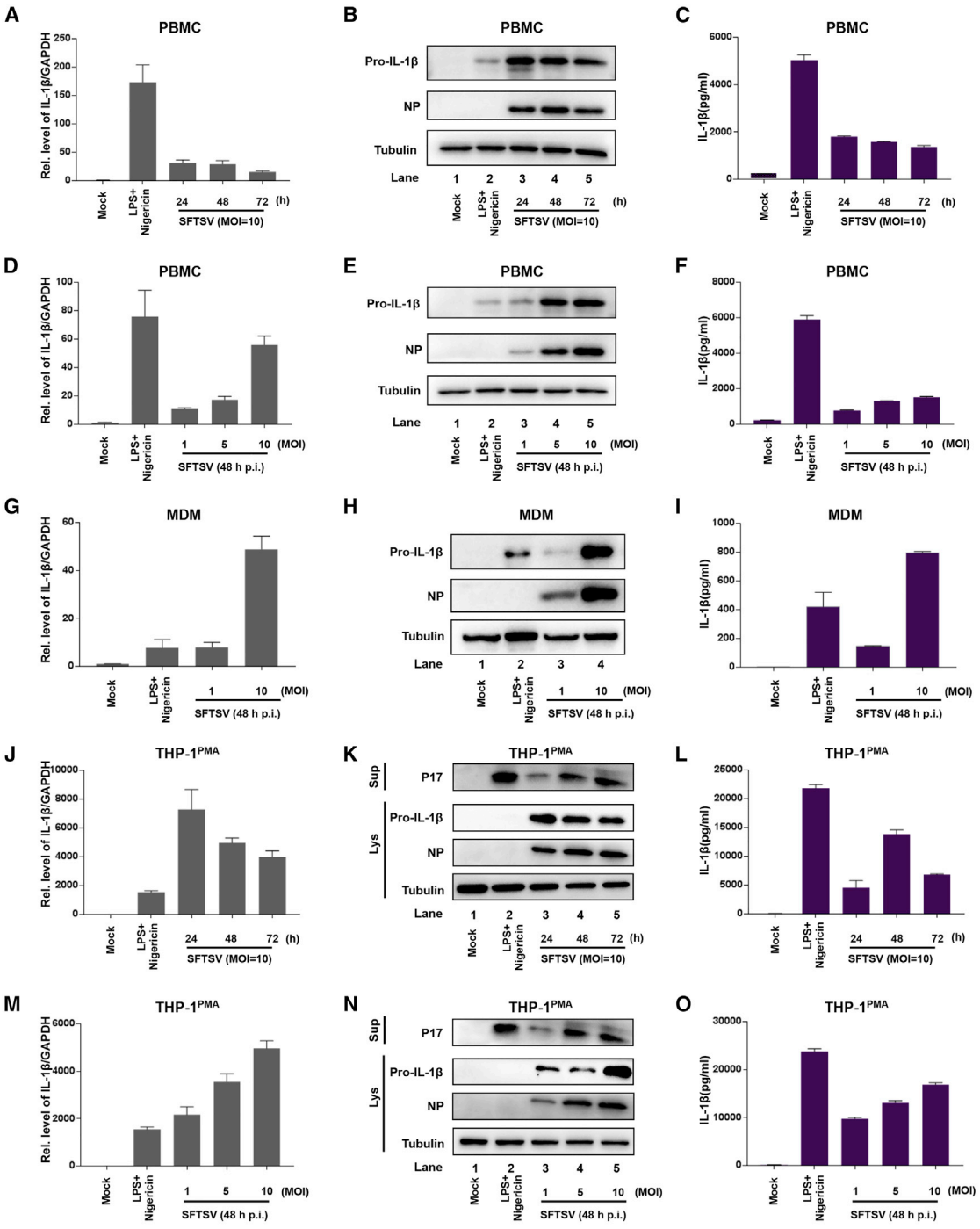

Figure 2. SFTSV Infection Stimulates IL-1β Production and Secretion

(A–C) PBMCs isolated from healthy donors were treated with LPS and nigericin, or infected with SFTSV with indicated time.

(A) Intracellular mRNA levels of *IL-1β* were measured with quantitative RT-PCR (qRT-PCR).

(B) Intracellular levels of pro-IL-1β were determined by western blot.

(C) Mature IL-1β levels in the supernatants were determined by ELISA.

(D–F) PBMCs were treated with LPS and nigericin, or infected with SFTSV with indicated MOI. Intracellular mRNA levels of *IL-1β* (D), intracellular levels of pro-IL-1β (E), mature IL-1β levels in the supernatants (F) were determined as above.

(G–I) MDMs were treated with LPS and nigericin or infected with SFTSV. *IL-1β* and *GAPDH* mRNAs (G), intracellular pro-IL-1β (H), and mature IL-1β levels in the supernatants (I) were determined as above.

(legend continued on next page)

pro-IL-1β both at the mRNA and the protein level (Figures 2A and 2B). ELISA analysis showed that SFTSV infection triggered IL-1β maturation and release in infected PBMCs (Figure 2C). When different MOIs were applied for virus infection, SFTSV infection triggered IL-1β maturation and release in a dose-dependent manner (Figures 2D–2F). Next, PBMCs were separated into monocyte and lymphocyte, and were analyzed for susceptibility of SFTSV infection. Monocyte is the main target cell in PBMCs (Figure S3A) and SFTSV induced IL-1β production in infected monocytes (Figures S3B–S3G), but not in lymphocytes (Figures S3H–S3J). We then prepared monocyte-derived macrophages (MDMs) from the purified monocytes and infected the MDMs with SFTSV. SFTSV infection of MDMs induced IL-1β maturation and release in a virus dose-dependent manner (Figures 2G–2I). Similar with human primary monocyte and MDMs, SFTSV infection of THP-1 cell, a human monocytic cell line, induced IL-1β production and maturation in a virus dose-dependent manner (Figures S4A–S4F). Finally, phorbol-12-myristate-13-acetate (PMA)-differentiated THP-1 macrophages (THP-1^{PMA}), a cell model of human macrophage, were tested. Similar with the above tested cell types, SFTSV infection of THP-1^{PMA} cells led to increased pro-IL-1β expression (Figures 2J and 2K) and triggered IL-1β maturation and release (Figure 2L). SFTSV infection of THP-1^{PMA} cells also resulted in a dose-dependent activation of IL-1β (Figures 2M–2O). Other inflammatory factors, such as IL-6 and TNF-α, were analyzed in SFTSV-infected THP-1^{PMA} cells, and these factors were upregulated similarly with IL-1β during SFTSV infection (Figures S4G–S4L). UV inactivation abolished SFTSV-induced IL-1β maturation and release in these cell types (Figure S5). Collectively, these results showed that SFTSV infection can induce inflammation activation in both SFTS patients and multiple inflammatory cell models.

SFTSV Infection Triggers the NF-κB Pathway through the TLR8-MyD88 Axis

Inflammation induction undergoes the "priming" and "activation" events of which the "priming" event stimulates upregulation of pro-IL-1β through the nuclear factor κB (NF-κB) pathway (Gross et al., 2011). Proteomic analysis of SFTSV-infected cells revealed strong NF-κB activation (Figure 3A). To analyze whether the SFTSV-induced pro-IL-1β upregulation is dependent on NF-κB activation, we added the NF-κB inhibitor, MLN120B, during SFTSV infection of THP-1^{PMA} cells. MLN120B treatment strongly inhibited induction of pro-IL-1β both at the mRNA and the protein level (Figures 3B and 3C), confirming that SFTSV induced pro-IL-1β upregulation through NF-κB activation. To determine how SFTSV activates the NF-κB pathway, we assessed the requirement for known signaling adaptor proteins in the activation of pro-IL-1β expression. The requirement for mitochondrial antiviral signaling protein (MAVS, also known as VISA, IPS-1, or Cardif) or myeloid differentiation primary response gene 88 (MyD88) for IL-1β expression was first analyzed. Knockdown of MyD88 potently abolished pro-IL-1β induction during SFTSV infection (Figures 3D and 3E). Also, ELISA analysis showed that IL-1β maturation and release induced by SFTSV infection were severely inhibited in MyD88-depleted cells (Figure 3F). In contrast, depletion of MAVS did not affect SFTSV-induced pro-IL-1β upregulation or IL-1β maturation and release (Figures 3D–3F). These results suggest that MyD88 plays a pivotal role in SFTSV-induced NF-κB activation, which is consistent with a recent study (Yamada et al., 2018).

It was recently reported that SFTSV enters cells through endocytosis (Liu et al., 2019). The role of MyD88 in mediating NF-κB activation during SFTSV infection suggests that the sensing event may happen in the endosome during virus entry. Consistent with early sensing during virus entry, the IL-1β mRNA level peaked at 2 h p.i. in SFTSV-infected cells (Figure S6A). The ligands of MyD88 in the endosome are Toll-like receptor 7 (TLR7) or TLR8, and both ligands recognize single-stranded RNA of invading pathogens (Majer et al., 2017). To identify the potential ligand recognizing viral RNA (vRNA), TLR7 or TLR8 was depleted in THP-1 through stable expression of short hairpin RNAs (shRNA) (Figures S6B and S6C). TLR8 depletion did not affect viral replication (Figure 3H; Figure S6D), but the expression of pro-IL-1β was significantly reduced (Figures 3G and 3H) concomitantly with reduced IL-1β maturation and release (Figure 3I). TLR7 depletion also significantly inhibited SFTSV-induced IL-1β maturation and release (Figures S6E–S6H). Unexpectedly, TLR7 depletion strongly inhibited SFTSV replication (Figures S6E and S6G), and therefore the reduced IL-1β induction could be because of reduced viral entry/replication. Notably, even though TLR7 depletion significantly inhibited SFTSV replication, the inhibition of IL-1β processing and release (Figure S6F) was less pronounced than in the TLR8-depleted cells, indicating that TLR8 plays a more important role in SFTSV-induced NF-κB activation. Taken together, these results suggest that the viral RNA triggers NF-κB pathway activation through the TLR8-MyD88 axis during virus entry.

SFTSV Infection Triggers the NLRP3 Inflammasome Activation

After the "priming" event, inflammasomes are activated and trigger proteolytic cleavage of dormant procaspase-1 into active caspase-1 to convert the precursor pro-IL-1β into mature and biologically active IL-1β (He et al., 2016). To determine the inflammasome mediating SFTSV-triggered IL-1β maturation and release, the caspase-1 activity was first assessed in SFTSV-infected cells. SFTSV infection of THP-1^{PMA} cells resulted in enhanced caspase-1 activity in an MOI-dependent manner (Figures 4A and 4B), indicating the involvement of caspase-1. Detection of caspase-1 maturation fragment (P20) confirmed activation of caspase-1 during SFTSV infection (Figure S7A).

(J–L) THP-1^{PMA} cells were treated with LPS and nigericin or infected with SFTSV with indicated time. Intracellular mRNA of *IL-1β* (J), P17 in supernatants or intracellular pro-IL-1β (K), and mature IL-1β in the supernatants (L) were determined as above.
(M–O) THP-1^{PMA} cells were treated with LPS and nigericin or infected with SFTSV with indicated MOI. Intracellular mRNA of *IL-1β* (M), P17 in supernatants or intracellular pro-IL-1β (N), and mature IL-1β in the supernatants (O) were determined as above. Data shown are means ± SD.
See also Figures S3–S5.

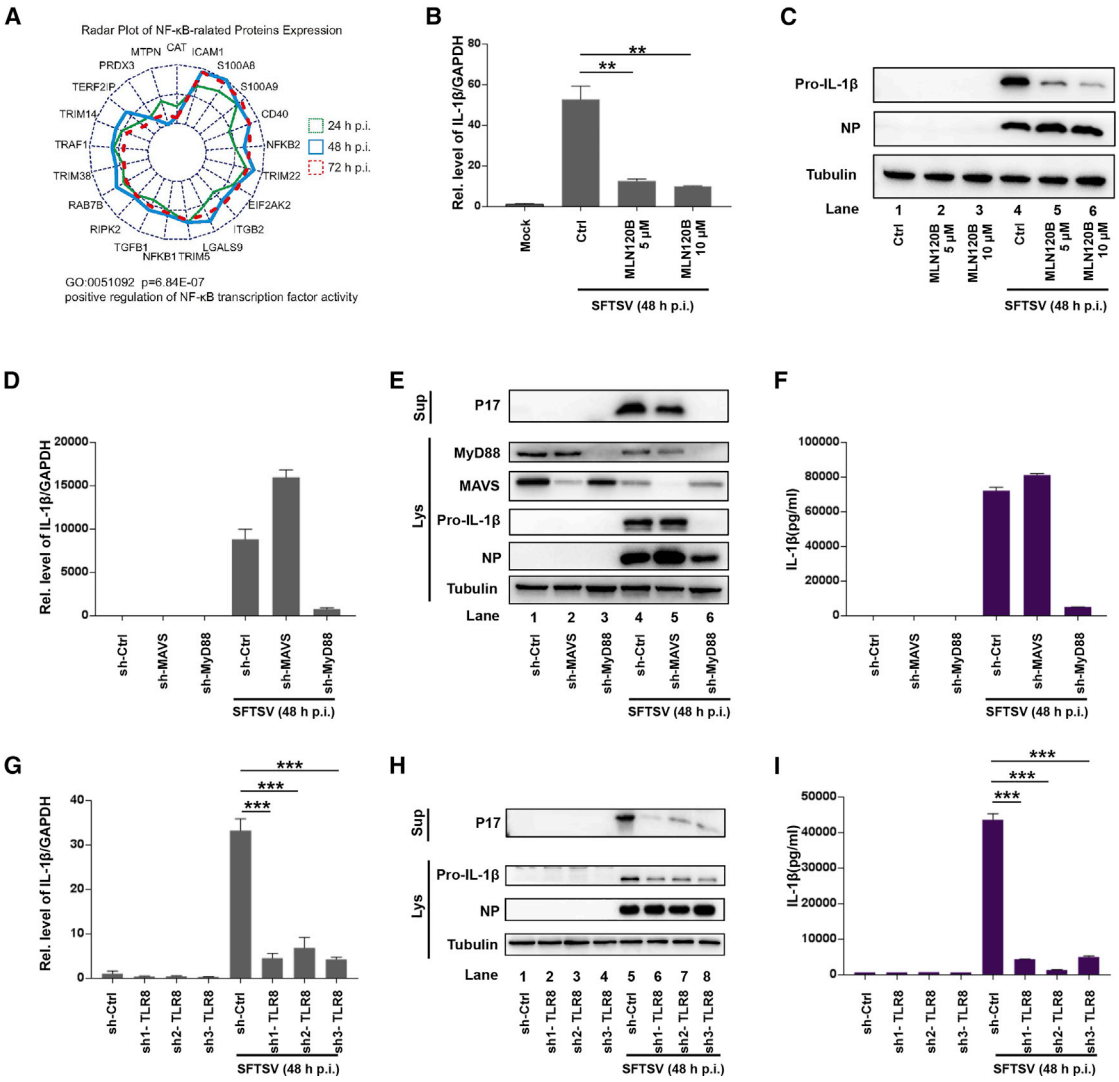

Figure 3. SFTSV Stimulates IL-1β Production through the Activation of the TLR8-MyD88-NF-κB Signaling Pathway

(A) Radar plot of the expression of proteins involved in "positive regulation of NF-κB transcription factor activity" at 24, 48, and 72 h p.i.

(B and C) THP-1^{PMA} cells were pre-treated with MLN120B and infected with SFTSV. Intracellular mRNA levels of *IL-1β* and *GAPDH* were measured with qRT-PCR (B). Intracellular pro-IL-1β was determined by western blot (C).

(D–F) THP-1^{PMA} cells stably expressing non-targeting shRNA (control) or specific shRNAs were mock treated or infected with SFTSV. Intracellular mRNA levels of *IL-1β* (D), P17 levels in the supernatants or pro-IL-1β levels in lysates (E), or IL-1β levels in the supernatants (F) were determined as above.

(G–I) THP-1^{PMA} cells stably expressing non-targeting shRNA (control) or specific shRNAs against TLR8 were mock treated or infected with SFTSV. Intracellular mRNA levels of *IL-1β* (G), P17 levels in supernatants or pro-IL-1β levels in lysates (H), and IL-1β levels in supernatants (I) were determined as above.

Comparison of mean values (B, G, and I) between two groups was analyzed by Student's t test. Data shown are means ± SD. $^{**}p < 0.01$; $^{***}p < 0.001$. See also Figure S6.

UV inactivation abolished SFTSV replication, caspase-1 maturation, and IL-1β release (Figure S7B). Treatment with VX-765, a caspase-1-specific inhibitor, reduced IL-1β maturation and release in lipopolysaccharide (LPS)- and nigericin-treated cells (Figures 4C and 4D), and also in SFTSV-infected cells (Figures 4E and 4F). Notably, the virus induced pro-IL-1β upregulation or viral infection was unaffected by VX-765 treatment (Figure 4E; Figure S7C). These results confirmed that SFTSV replication-induced inflammation activation depends on caspase-1 activity. ASC is an inflammasome adaptor protein, and its oligomerization is an indicator of inflammasome activation (Lamkanfi and Dixit, 2014). To analyze whether SFTSV infection induced ASC oligomerization, we infected THP-1^{PMA} cells with SFTSV, and the cell pellet was harvested and cross-linked as previously described (He et al., 2018; Wang et al., 2018). Oligomerization of ASC was observed in the cell pellet of LPS- and nigericin-treated cells, as well as in SFTSV-infected cells, but not in mock-infected cells (Figure 4G), confirming the involvement of ASC oligomerization in the formation of the SFTSV-activated inflammasome.

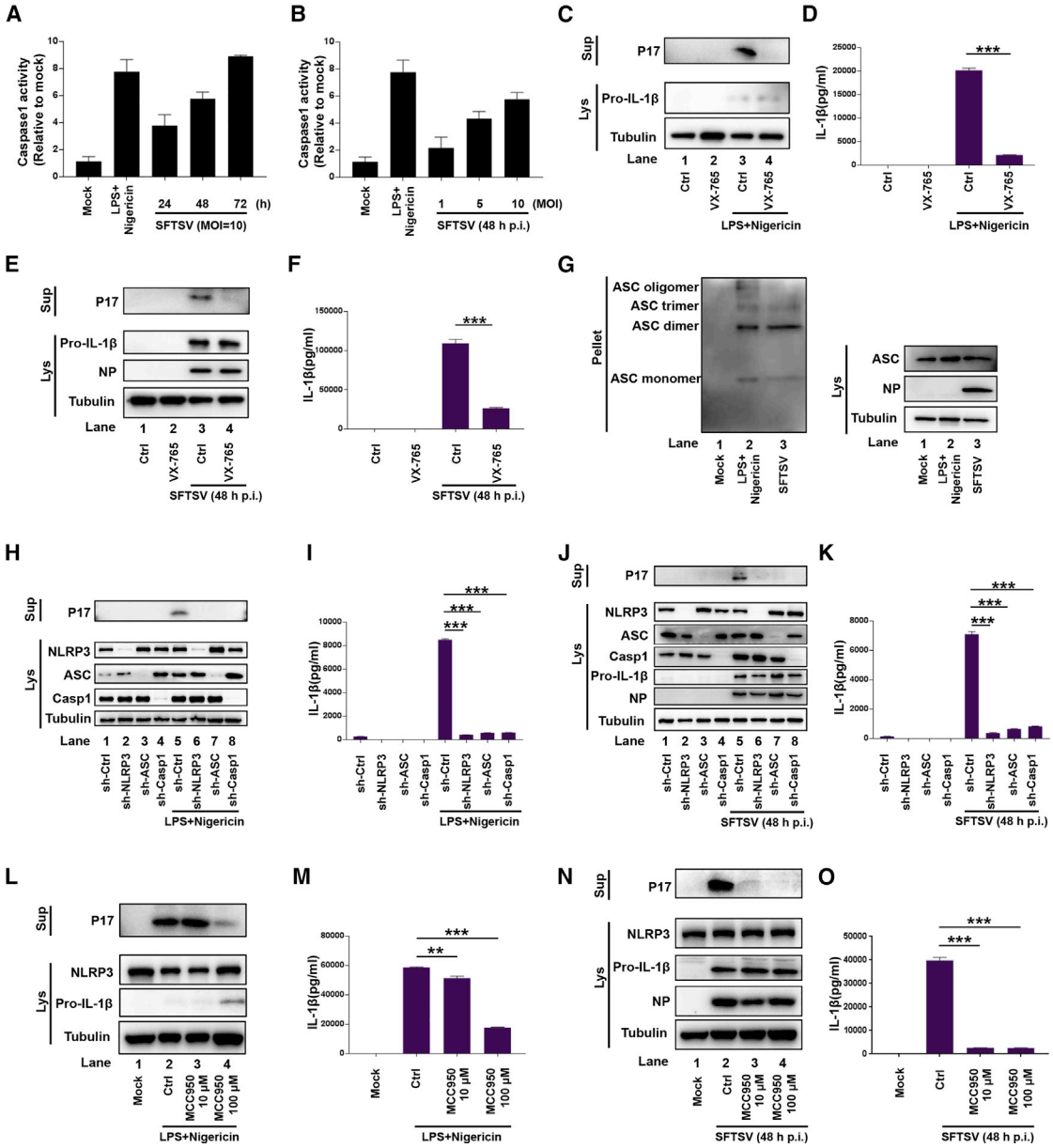

Figure 4. The Role of NLRP3 Inflammasome in IL-1β Secretion Induced by SFTSV Infection

(A and B) THP-1^{PMA} cells were treated with LPS and nigericin or infected with SFTSV with indicated time (A) and MOI (B). Caspase-1 activity in lysates was determined.

(C and D) THP-1^{PMA} cells were treated with caspase-1 inhibitor VX-765 followed by LPS and nigericin treatment. (C) P17 in supernatants or pro-IL-1β in lysate was determined by western blot. (D) IL-1β levels in supernatants were determined by ELISA.

(E and F) THP-1^{PMA} cells were treated with VX-765 followed by SFTSV infection (MOI = 10). P17 in supernatants or pro-IL-1β in lysate (E) and IL-1β levels in supernatants (F) were determined as above.

(G) THP-1^{PMA} cells were treated with LPS and nigericin or infected with SFTSV at an MOI of 10 for 48 h. ASC oligomerization was determined by western blot.

(H and I) THP-1^{PMA} cells stably expressing non-targeting shRNA (control) or specific shRNAs were treated with LPS and nigericin. P17 in supernatants or pro-IL-1β in lysates (H) and IL-1β levels in supernatants (I) were determined as above.

(J and K) THP-1^{PMA} cells stably expressing non-targeting shRNA or specific shRNAs were infected with SFTSV at an MOI of 10. P17 in supernatants or pro-IL-1β in lysates (J) and IL-1β levels in supernatants (K) were determined as above.

(L and M) THP-1^{PMA} cells were pre-treated with NLRP3 inhibitor MCC950 followed by LPS and nigericin treatment. P17 in supernatants or pro-IL-1β in lysates (L) and IL-1β levels in supernatants (M) were determined as above.

(N and O) THP-1^{PMA} cells were pre-treated with MCC950 followed by SFTSV infection (MOI = 10). P17 in supernatants or pro-IL-1β in lysates (N) and IL-1β levels in supernatants (O) were determined as above.

Comparison of mean values (D, F, I, K, M, and O) between two groups was analyzed by Student's t test. Data shown are means ± SD. $^{**}p < 0.01$; $^{***}p < 0.001$. See also Figure S7.

NLRP3 inflammasome was reported to be associated with inflammation responses triggered by several RNA viruses (Chen and Ichinohe, 2015); therefore, we analyzed its potential role in SFTSV-induced inflammation. NLRP3, caspase-1, and ASC were depleted in THP-1 cells, respectively, and western blot analysis confirmed the silencing of these genes (Figure 4H). Next, differentiated macrophages from these cells were treated with LPS and nigericin, or infected with SFTSV followed by analysis of IL-1β maturation and release. Whereas treatment with LPS and nigericin induced potent IL-1β maturation and release in control cells, depletion of these proteins strongly impaired IL-1β maturation and release as previously reported (Figures 4H and 4I; Wang et al., 2018). SFTSV infection of control cells also induced potent IL-1β maturation and release (Figures 4J and 4K). Depletion of NLRP3, ASC, or caspase-1 did not reduce SFTSV infection or induction of pro-IL-1β expression (Figure 4J; Figure S7D). However, IL-1β maturation and release were abolished in these cells, indicating involvement of NLRP3 inflammasome in SFTSV-induced inflammatory responses (Figures 4J and 4K). Treatment with MCC950, a potent NLRP3-specific inhibitor, significantly inhibited IL-1β maturation and release in THP-1^{PMA} cells treated with LPS and nigericin (Figures 4L and 4M) or infected by SFTSV without affecting SFTSV-induced pro-IL-1β upregulation or viral infection (Figures 4N and 4O; Figure S7E). Taken together, these results suggest that SFTSV infection induced NLRP3 inflammasome activation to trigger IL-1β maturation and release.

SFTSV Infection Induces Mitochondrial Damage and mtROS Production

Multiple different stimuli trigger NLRP3 inflammasome activation, and it was recently proposed that these different stimuli trigger NLRP3 inflammasome activation through inducing mitochondrial dysfunction (He et al., 2016). Comparison of the transcriptomic and proteomic analyses showed consistent regulation of multiple pathways, including inflammation response, type I IFN signaling pathway, cell adhesion, etc. However, different regulation of mitochondrial proteins in these two analyses was observed: while transcriptomic analysis revealed upregulation of mRNAs of mitochondrial proteins, proteomic analysis showed downregulation of the majority of mitochondrial proteins in SFTSV-infected cells (Figures 5A and 5B), indicating mitochondrial dysfunction during SFTSV infection. Western blot analysis of representative mitochondrial proteins confirmed the reduction of protein abundance (Figure S2D, lower panel). We therefore assessed whether SFTSV infection led to mitochondrial dysfunction. mtROS production and/or loss of mitochondrial membrane potential is associated with mitochondrial dysfunction (Shadel and Horvath, 2015), and we first analyzed whether SFTSV infection can lead to mtROS production. THP-1^{PMA} cells were infected with SFTSV with an increasing amount of viral dose and stained with MitoSOX, an indicator dye for highly selective detection of superoxide in the mitochondria (Lai et al., 2018). Nigericin treatment was included as the positive control (Chung et al., 2018). SFTSV infection induced mtROS production in infected cells in a dose-dependent manner, and UV inactivation abolished SFTSV-induced mtROS production (Figure 5C). Next, the mitochondrial membrane potential ($\Delta\psi_m$) was measured by tetramethyl rhodamine methyl ester (TMRM) incorporation assay (Shimada et al., 2012). THP-1^{PMA} cells were infected with an increasing amount of viral dose, and treatment with carbonyl cyanide 3-chlorophenylhydrazone (CCCP) was included as the positive control as previously described (Soutar et al., 2019). As shown in Figures 5D and 5E, $\Delta\psi_m$ was reduced in SFTSV-infected THP-1^{PMA} cells in an MOI-dependent manner, whereas UV inactivation prevented SFTSV-induced $\Delta\psi_m$ reduction (Figure 5F). Taken together, these results showed that SFTSV infection induced mtROS production and loss of mitochondrial membrane potential.

SFTSV Infection Induces mtDNA Release to Trigger NLRP3 Inflammasome Activation

Mitochondrial dysfunction is often associated with mtDNA oxidization and release into the cytosol, and the released mtDNA can stimulate NLRP3 inflammasome activation (He et al., 2016; Shimada et al., 2012; Zhong et al., 2018). We therefore analyzed whether SFTSV infection induced mtDNA release into the cytosol. First, the amount of total intracellular mtDNA was measured in SFTSV-infected or control THP-1^{PMA} cells, and SFTSV infection did not affect the amount of total mtDNA (Figure 6A). Next, the cytosolic extracts were prepared from SFTSV-infected and mock cells, and the separation of cytosolic fragmentation was verified (Figure S9A). Quantification analysis of cytosolic mtDNA revealed a significant increase of cytosolic mtDNA in the SFTSV-infected cells compared with the mock control (Figure 6A), suggesting that SFTSV infection induced release of mtDNA into the cytosol. SFTSV infection of primary human monocytes also resulted in cytosolic mtDNA release (Figure 6B).

To address whether the released cytosolic mtDNA was bound with NLRP3, we performed co-immunoprecipitation analysis with NLRP3 antibody and quantified the amount of associated mtDNA with quantitative PCR (qPCR) analysis. 5-Bromo-2′-deoxyuridine (BrdU) was added to SFTSV-infected or mock cells for detection of mtDNA as previously described (Shimada et al., 2012; Zhong et al., 2018). Dot blot analysis with BrdU antibody revealed the association between mtDNA and NLRP3 in LPS- and nigericin-treated or SFTSV-infected cells, but not in mock-infected cells (Figure 6C). qPCR analysis confirmed the significantly enhanced association between mtDNA and NLRP3 in SFTSV-infected cells compared with the mock control (Figure 6D). Next, we analyzed whether mtDNA colocalized with NLRP3 inflammasome in infected cells. Staining with NLRP3 antibody showed a largely diffusive distribution of NLRP3 in mock cells but revealed speck-like NLRP3 structures in infected cells, indicating formation of NLRP3 inflammasome (Figure S8A). We also used 5-ethynyl-2′-deoxyuridine (EdU) to label mtDNA and analyzed its cellular localization in SFTSV-infected cells. EdU is another thymidine analog that can be incorporated into newly synthesized DNA and is more amenable for fluorescence microscopy analysis (Salic and Mitchison, 2008). EdU has been successfully used to label mtDNA to study its association with inflammasome (Zhong et al., 2018). Cytoplasmic EdU signals representing mtDNA displayed distinct co-localization with NLRP3 specks in SFTSV-infected cells, whereas in mock cells, no co-localization between mtDNA signal and NLRP3

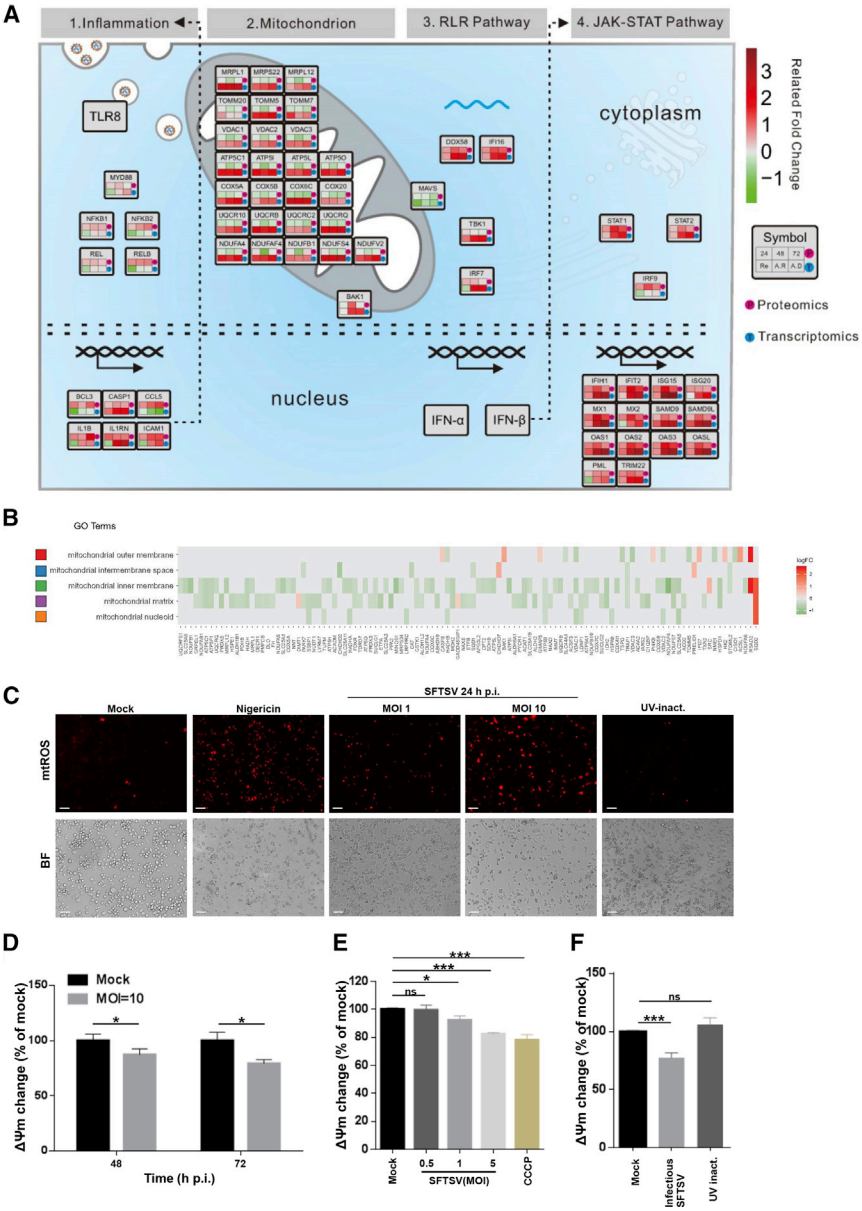

Figure 5. SFTSV Infection Induced Mitochondrial Damage

(A) Comparative transcriptomic and proteomic analyses reveal downregulation of mitochondrial proteins during SFTSV infection. Selected biological processes regulated by SFTSV infection are displayed. Results from both transcriptomic and proteomic analyses were shown for each gene (indicated by the box). For each gene, the three upper boxes contain proteomics data from three time points, and the three lower boxes contain patient transcriptomic data. Red: upregulation; green: downregulation.

(B) Intracellular levels of mitochondrial proteins in SFTSV-infected cells at 48 h p.i. GO analysis based on cellular component grouped mitochondrial proteins into five categories (denoted to the left of the panel). Relative intracellular levels of mitochondrial proteins were determined by quantitative proteomic. Red: upregulated; green: downregulated.

(C) THP-1^{PMA} cells were treated with nigericin, infected with SFTSV, or inoculated with UV-inactivated SFTSV. Intracellular mtROS was stained with MitoSOX (red). Scale bars represent 50 μm.

(D–F) THP-1^{PMA} cells were infected with SFTSV with indicated MOI and time (D), treated with CCCP (E), or inoculated with UV-inactivated SFTSV for 48 h (F). Changes in ΔΨm were measured by staining cells with the TMRM probe. Comparison of mean values (D–F) between two groups was analyzed by Student's t test. Data shown are means ± SD. *$p < 0.05$; ***$p < 0.001$. BF, bright field; ns, no significance. See also Figure S2.

was detected (Figure 6E). These results confirmed the association between mtDNA and NLRP3 inflammasome induced by SFTSV infection.

It was recently reported that the oxidized form of mtDNA (ox-mtDNA) is a more potent trigger of NLRP3 activation (Shimada et al., 2012). SFTSV infection induced mtROS production, suggesting that the released mtDNA might be in the oxidized form to trigger NLRP3 activation. To analyze this, THP-1^{PMA} cells infected with SFTSV were lysed and subjected to co-immunoprecipitation with NLRP3 antibody. Precipitated samples were probed with antibody against 8-hydroxy-guanosine (8-OH-dG), which can be used to detect oxidized DNA (Shimada et al., 2012; Zhong et al., 2018). Dot blot analysis with 8-OH-dG antibody showed that the mtDNA precipitated by NLRP3 antibody in LPS- and nigericin-treated or SFTSV-infected cells was present in the oxidized form (Figure 6F). Next, the SFTSV-infected or mock-treated THP-1^{PMA} was labeled with 8-OH-dG antibody and analyzed with immunofluorescence microscopy. Labeling with 8-OH-dG antibody revealed more distinct 8-OH-dG punctate signals in the cytoplasm of SFTSV-infected cells, but showed only weak and irregular signals in control cells (Figure S8B). Furthermore, SFTSV-infected or mock cells were probed with 8-OH-dG and NLRP3 antibodies, and a distinct co-localization between punctate ox-mtDNA signal and NLRP3 speck was observed in the cytoplasm of SFTSV-infected cells, but not in mock cells (Figure 6G; Figures S8C and S8D). This suggests that the cytoplasmic ox-mtDNA binds NLRP3 inflammasome in SFTSV-infected cells.

To further verify the role of mtDNA in activation of NLRP3 inflammasome during SFTSV infection, we treated THP-1 cells with ethidium bromide (EtBr), which results in mtDNA depletion and is often used to study the role of mtDNA in regulation of innate immunity (Dang et al., 2017; Rongvaux et al., 2014). EtBr treatment led to significant reduction of total intracellular mtDNA compared with the control treatment (Figure S9B). Also, the amount of cytosolic mtDNA in SFTSV-infected cells

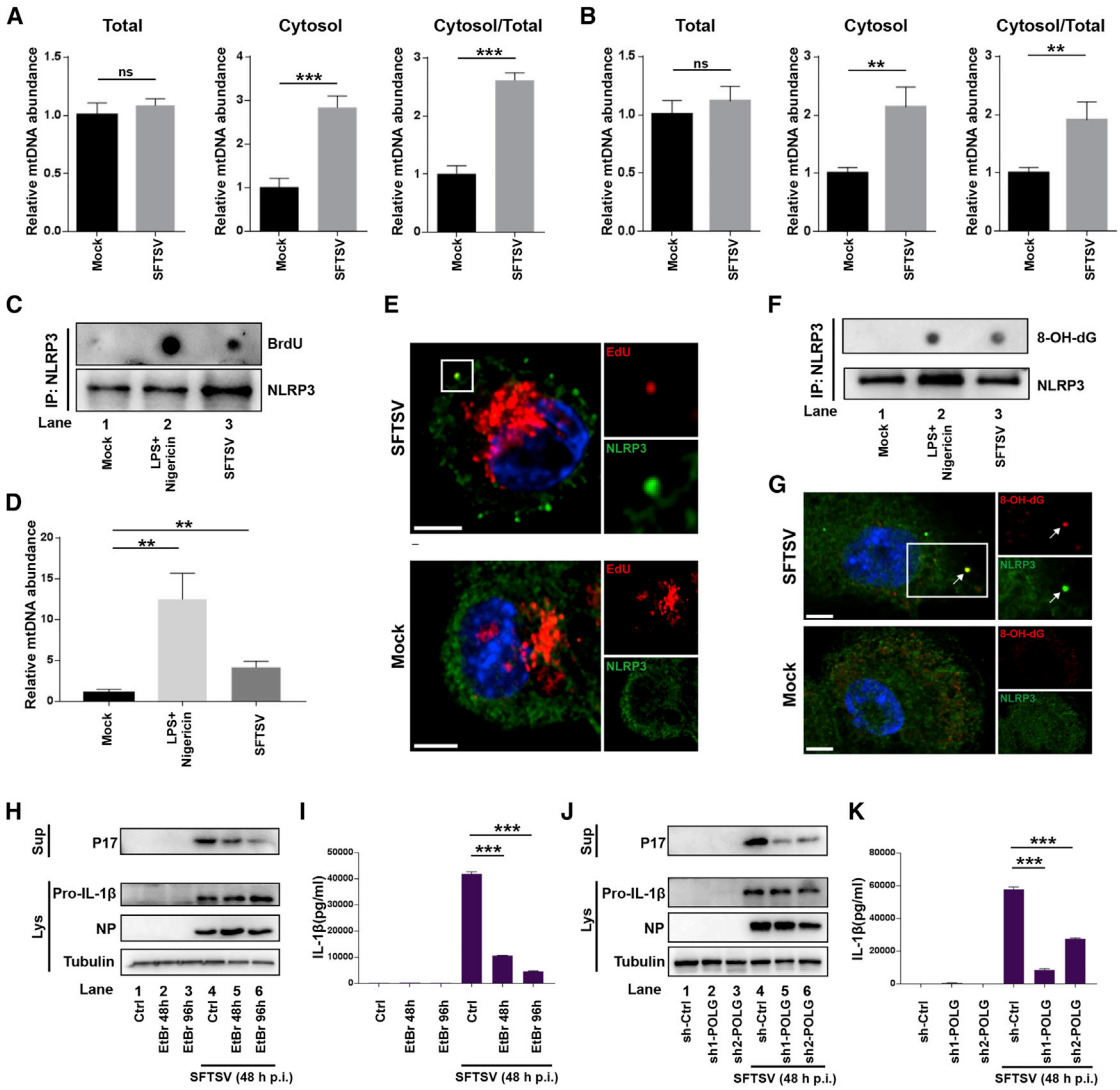

Figure 6. SFTSV-Induced mtDNA Release Triggers NLRP3 Inflammasome Activation

(A and B) THP-1^{PMA} cells (A) or primary human monocytes (B) infected with SFTSV (MOI = 10) for 24 h were collected, and total or cytosolic DNA was extracted. Total or cytosolic mtDNA levels were determined with qPCR.

(C) THP-1^{PMA} cells were pre-loaded with BrdU, treated with LPS and nigericin, or infected with SFTSV at an MOI of 10 for 24 h. Cell lysates were collected and immunoprecipitated with anti-NLRP3 Ab, then detected by dot blots probed with anti-BrdU Ab.

(D) mtDNA bound to NLRP3 was determined via immunoprecipitation of NLRP3 followed by qPCR analysis of mtDNA.

(E) EdU-labeled THP-1^{PMA} cells were co-stained for NLRP3, EdU, and DAPI at 24 h postinfection (MOI = 10). Box shows co-localization of EdU and NLRP3 signals. Scale bars represent 5 μm.

(F) THP-1^{PMA} cells were treated with LPS and nigericin or infected with SFTSV as above. Cell lysates were collected and immunoprecipitated with anti-NLRP3 Ab, then dot blotted with anti-8-OH-dG Ab.

(G) THP-1^{PMA} cells were co-stained for NLRP3, 8-OH-dG, and DAPI at 24 h after SFTSV infection. Arrow indicates co-localization of 8-OH-dG and NLRP3 signals. Scale bars represent 5 μm.

(H and I) THP-1^{PMA} cells were pre-treated with EtBr and then mock treated or infected with SFTSV (MOI = 10). P17 in supernatants or pro-IL-1β in lysates was determined by western blot (H). IL-1β levels in supernatants were determined by ELISA (I).

(J and K) THP-1^{PMA} cells stably expressing non-targeting shRNA (control) or specific shRNAs were mock treated or infected with SFTSV. P17 in supernatants or pro-IL-1β in lysates (J) and IL-1β levels in supernatants (K) were determined as above.

Comparison of mean values (A, B, D, I, and K) between two groups was analyzed by Student's t test. Data shown are means ± SD. **$p < 0.01$; ***$p < 0.001$; ns, no significance. See also Figures S8–S10.

was significantly reduced in EtBr-treated cells compared with control cells (Figure S9C). Compared with the control-treated cells, SFTSV-induced IL-1β maturation and release were significantly reduced in EtBr-treated cells as revealed by both western blot and ELISA analyses, whereas pro-IL-1β upregulation and viral replication were unaffected (Figures 6H and 6I; Figure S9D). Depletion of mtDNA in THP-1 cells was also attempted through knockdown of DNA polymerase gamma (POLG), which is the mitochondrion DNA polymerase responsible for mtDNA synthesis (Krasich and Copeland, 2017). POLG depletion (Figure S9E) led to significant reduction of total mtDNA (Figure S9F) and also reduced the amount of mtDNA released into the cytosol upon SFTSV infection (Figure S9G). Similar with EtBr-treated cells, SFTSV-induced IL-1β maturation and release were significantly reduced in POLG-depleted cells, whereas pro-IL-1β induction or viral replication was unaffected (Figures 6J and 6K; Figure S9H). To analyze whether oxidization of mtDNA is important for SFTSV-induced NLRP3 inflammasome activation, we added Mito-TEMPO, a specific scavenger of mitochondrial superoxide to reduce mtDNA oxidization (Lai et al., 2018), during SFTSV infection. Addition of Mito-TEMPO reduced SFTSV-induced IL-1β maturation and release in a dose-dependent manner (Figures S9I and S9J). Furthermore, addition of 8-OH-dG, which can complete the interaction between ox_mtDNA and NLRP3 (Shimada et al., 2012), also resulted in reduced IL-1β maturation and release during SFTSV infection (Figures S9K and S9L). These results together suggest that SFTSV infection leads to mtDNA oxidization and release, and the cytosolic ox-mtDNA binds and triggers NLRP3 inflammasome activation.

SFTSV-Induced mtDNA Release Is an Upstream Event of NLRP3 Inflammasome Activation

It is debatable whether mtDNA release is an upstream event triggering NLRP3 inflammasome activation or, instead, NLRP3 inflammasome activation leads to mtDNA release (He et al., 2016). To delineate this in the context of SFTSV infection, we added the NLRP3-specific inhibitor MCC950 during SFTSV infection and analyzed the mtDNA release and IL-1β maturation. Although addition of MCC950 strongly blocked SFTSV-induced NLRP3 inflammasome activation, the amount of mtDNA released into the cytosol was comparable between MCC950-treated and control cells (Figures S10A and S10B). MCC950 treatment also did not affect the amount of total cellular mtDNA (Figure S10C). Release of mtDNA was further analyzed in NLRP3-depleted cells. Whereas NLRP3 depletion inhibited IL-1β maturation and release triggered by SFTSV infection (Figure S10D), virus infection-induced mtDNA release was comparable with the control cells (Figure S10E). Also, NLRP3 depletion did not affect the amount of total cellular mtDNA (Figure S10F). These results together suggested that the SFTSV infection-induced mtDNA release is an upstream event that precedes NLRP3 inflammasome activation.

SFTSV-Induced BAK/BAX Activation Facilitates mtDNA Release

We next investigated the mechanism of SFTSV-induced mtDNA release. Proteomic analysis showed that although the majority of mitochondrial proteins were downregulated during SFTSV infection, the mitochondrial protein BCL2 antagonist/killer 1 (BAK) was significantly upregulated (Figure 7A). Both qPCR and western blot analysis confirmed BAK upregulation in SFTSV-infected THP-1^{PMA} (Figures 7B and 7C). BAK together with BCL2-associated X (BAX) mediate mitochondrial outer membrane permeabilization (MOMP) (Galluzzi and Vanpouille-Box, 2018), which may lead to mitochondrial inner membrane herniation into the cytosol followed by mtDNA release (McArthur et al., 2018; Riley et al., 2018). A downstream event of BAK/BAX activation is the release of cytochrome *c* into the cytosol (Galluzzi and Vanpouille-Box, 2018). To analyze whether SFTSV infection induces BAK/BAX activation, we prepared cytosolic fractions of SFTSV-infected or control THP-1^{PMA} and analyzed the amount of cytosolic cytochrome *c*. Compared with the mock cell, the amount of cytosolic cytochrome *c* was higher in SFTSV-infected cells, indicating that SFTSV induced BAK/BAX activation (Figure 7D). We therefore examined whether BAK/BAX mediated mtDNA release during SFTSV infection. BAK or BAX depletion (Figures S11A and S11D) significantly reduced the amount of mtDNA released into the cytosol upon SFTSV infection (Figures 7E and 7H), but did not affect the amount of total cellular mtDNA (Figures S11B and S11E). Depletion of BAK or BAX did not affect virus replication or virus-induced pro-IL-1β production (Figures 7F and 7I; Figures S11C and S11F) but significantly reduced SFTSV-induced IL-1β maturation and release (Figures 7G and 7J). To further investigate whether upregulation of BAK led to BAK/BAX activation, we transfected HEK293T cells with an increasing amount of BAK expression plasmid and analyzed cytosolic mtDNA and cytochrome *c* release. Overexpression of BAK led to an increased amount of cytosolic cytochrome *c* and mtDNA release (Figures S11G–S11J), indicating BAK/BAX activation. These results together suggested that SFTSV infection-induced mtDNA release is dependent on BAK/BAX activation.

BAK Expression Level Correlates with SFTS Disease Progression and Fatal Outcome

Results from the transcriptomic analysis showed significant upregulation of BAK in SFTS patients compared with healthy controls, and the fatal SFTS patients had the highest BAK expression level (Figure 7K). Comparing virus titer in the acute infection stage of patients showed that the virus titer in fatal patients is higher than that in patients who eventually recovered from SFTSV infection (Figure 7L), consistent with SFTSV replication-induced BAK upregulation. To verify the potential correlation between BAK upregulation and fatal outcome, we collected blood samples from SFTS patients on different days during hospitalization and determined the BAK expression level. The SFTS patients were categorized into the group of "survival" or "fatal" according to their final clinical outcome. The patients who died of fatal infection (n = 5, red lines) showed significantly higher levels of BAK expression compared with patients who survived the SFTSV infection (n = 10, black lines) throughout the period of hospitalization (Figure 7M). Furthermore, both groups of SFTS patients showed higher levels of BAK expression compared with the healthy controls (n = 10, mean value, dashed line, Figure 7M). These results indicated that the BAK expression

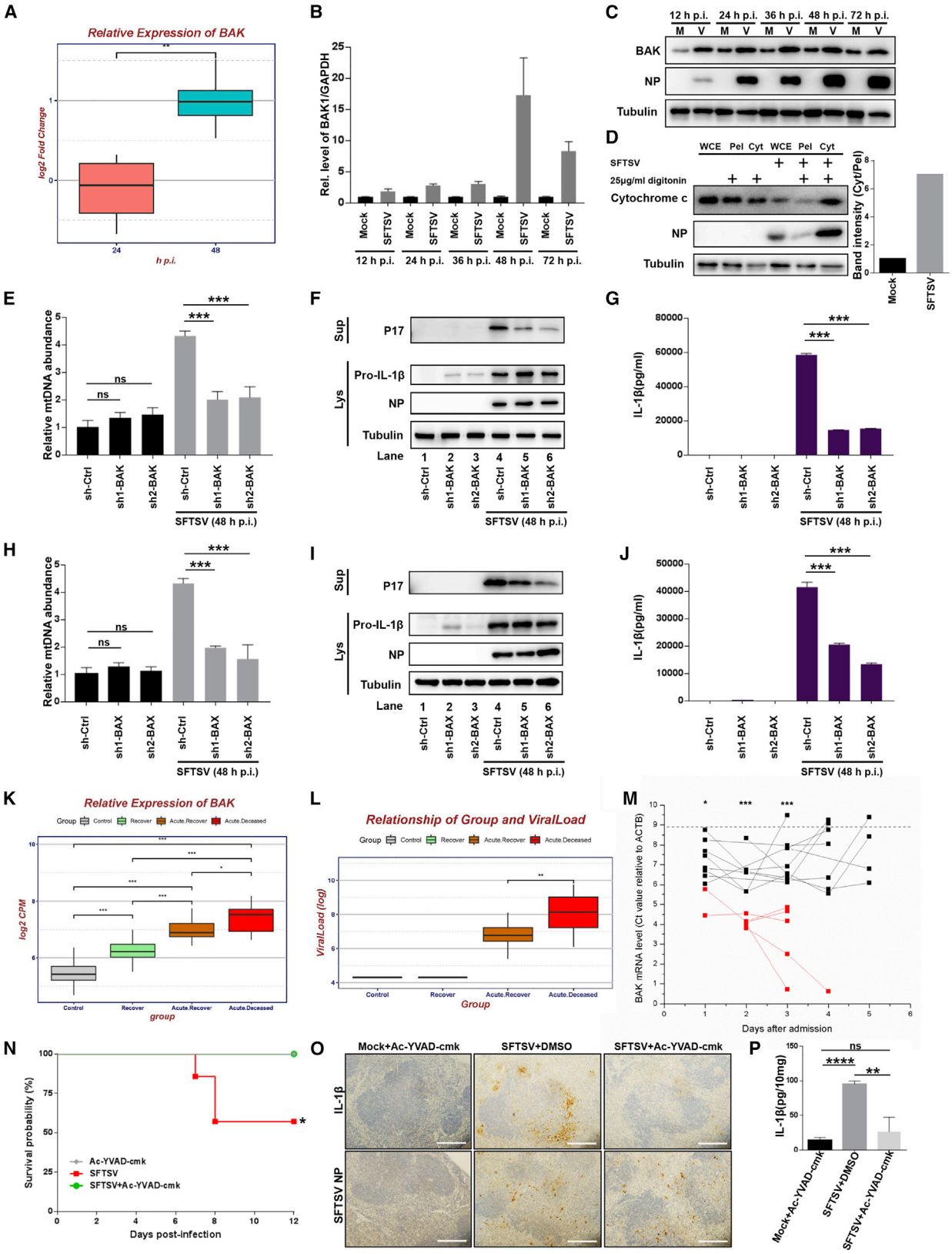

(legend on next page)

level is correlated with SFTS disease progression and fatal outcome.

SFTSV-Induced Inflammatory Response Is Associated with Fatal Infection in Mouse Model

Finally, the potential correlation between virus-induced inflammatory response and fatal outcome was analyzed in a lethal SFTSV mouse model (Lazear et al., 2016). C57BL/6 mice were treated with anti-IFNAR1 (interferon alpha/beta receptor 1) immunoglobulin G (IgG) and then challenged intraperitoneally with SFTSV. At 1 h p.i., mice were intraperitoneally injected with caspase-1 inhibitor (Ac-YVAD-cmk) (n = 8) or equal volume of DMSO (n = 7). Mice treated with DMEM and Ac-YVAD-cmk (n = 5) were included as the negative control. Ac-YVAD-cmk or DMSO was administered on a daily basis for 5 days, and the mice were monitored for 12 days. For detection of IL-1β, mice were similarly infected with SFTSV with or without Ac-YVAD-cmk treatment and at 5 days p.i., spleen samples were collected from mice treated with Ac-YVAD-cmk (n = 4) or DMSO (n = 3), and the IL-1β was detected by ELISA and immunohistochemistry staining. Mice treated with DMEM and Ac-YVAD-cmk (n = 3) were included as the negative control. SFTSV infection of anti-IFNAR1 IgG-treated mice led to a fatality rate of 42.9%, whereas Ac-YVAD-cmk treatment reduced production of IL-1β in the spleen (Figures 7O and 7P) and rescued the SFTSV-induced fatality ($p < 0.05$; Figure 7N). These results supported the notion that SFTSV replication-triggered inflammatory response is associated with fatal infection outcome.

DISCUSSION

Mitochondrion plays a critical role in innate immunity regulation through functioning as a signaling platform and/or exposing immune stimulatory mitochondrial damage-associated molecular patterns such as mtDNA (Dhir et al., 2018; Kanneganti et al., 2015). Here we show that SFTSV infection induces mtDNA release to bind and trigger NLRP3 inflammasome activation leading to disease-associated inflammatory responses. Recently, it was reported that new mtDNA synthesis is necessary for the production of oxidized mtDNA for NLRP3 inflammasome activation in the model of LPS-primed murine macrophages (Zhong et al., 2018). Notably, SFTSV infection of macrophages did not lead to significant synthesis of new mtDNA, but oxidized mtDNA was released into the cytosol and activated NLRP3 inflammasome. This suggests that oxidization of mtDNA can still occur in the absence of new mtDNA synthesis, and release of the oxidized mtDNA is the critical event in NLRP3 inflammation activation, at least in the context of SFTSV infection. This would also suggest that blocking mtDNA release could be a potential target for developing anti-inflammation therapeutic strategies against SFTSV infection.

The mechanism of mtDNA release is a topic under intense investigation, and recent studies suggested that BAK/BAX activation plays a pivotal role during this event (Galluzzi and Vanpouille-Box, 2018; McArthur et al., 2018; Riley et al., 2018). SFTSV-induced mtDNA release also depends on BAK/BAX because depletion of BAK or BAX significantly inhibited SFTSV-induced mtDNA release and concomitantly reduced IL-1β maturation and release. Upon activation, BAK/BAX form oligomers and mediate macropore formation on the mitochondrial outer membrane, resulting in mitochondrial inner membrane herniation into the cytosol and subsequently mtDNA release (McArthur et al., 2018; Riley et al., 2018). Transcriptomic analysis of samples from SFTS patients showed that virus infection led to pronounced BAK upregulation, and a correlation between BAK expression level and disease severity and fatality

Figure 7. SFTSV Infection Induces mtDNA Release through BAK/BAX Activation

(A) Intracellular BAK level in SFTSV-infected cells at 24 or 48 h p.i. determined by MS.

(B and C) THP-1^{PMA} cells were infected with SFTSV (MOI = 10) for indicated time. Relative mRNA levels of *BAK* were measured with qRT-PCR (B). BAK levels in lysates were determined by western blot (C).

(D) Mock-treated or SFTSV-infected (MOI = 10 for 24 h) THP-1^{PMA} cells were subjected to digitonin (25 μg/mL) fractionation, and whole-cell extracts (WCE), pellets (Pel), or cytosolic extracts (Cyt) were blotted with indicated Abs. Band intensity of cytochrome *c* was determined by ImageJ.

(E–G) THP-1^{PMA} cells stably expressing non-targeting shRNA or shRNAs against BAK were mock treated or infected with SFTSV (MOI = 10).

(E) Cytosolic mtDNA levels were quantified with qPCR.

(F) P17 in supernatants or pro-IL-1β in lysates was determined by western blot.

(G) IL-1β levels in supernatants were determined by ELISA.

(H–J) THP-1^{PMA} cells stably expressing non-targeting shRNA or shRNAs against BAX were mock treated or infected with SFTSV (MOI = 10). Cytosolic mtDNA levels (H), P17 in supernatants or pro-IL-1β in lysates (I), IL-1β levels in supernatants (J) were determined as above.

(K) Relative mRNA levels of BAK in four groups of patients quantified by transcriptomic analysis.

(L) Viral load in the serum of SFTS patients and healthy donors was quantified by qRT-PCR with the specific primers against the SFTSV NP (nucleoprotein) RNA.

(M) The comparison of *BAK* mRNA level between 5 fatal and 10 surviving SFTS cases. Whole blood cells from 5 fatal and 10 surviving SFTS cases were collected, and relative intracellular level of *BAK* mRNA was determined by qRT-PCR. Red: fatal SFTS cases; black: surviving SFTS cases; dashed line: cycle threshold (Ct) value of *BAK* mRNA from healthy donors. The Ct value of *BAK* was normalized to *ACTB*.

(N) The effect of caspase-1 inhibitor on SFTSV-induced fatality in mice. C57BL/6 mice pretreated with anti-IFNAR1 IgG were intraperitoneally inoculated with SFTSV and treated with DMSO or Ac-YVAD-cmk by intraperitoneal injection. The mice were monitored for 12 days, and survival rates were evaluated. Comparison of survival curves between anti-IFNAR1 SFTSV and anti-IFNAR1 SFTSV Ac-YVAD-cmk was analyzed by log rank (Mantel-Cox) test. *$p < 0.05$.

(O and P) The effect of caspase-1 inhibitor on SFTSV-induced IL-1β production in the mouse spleen. C57BL/6 mice pretreated with anti-IFNAR1 IgG were intraperitoneally inoculated with SFTSV and treated with DMSO or Ac-YVAD-cmk by intraperitoneal injection. Mice treated with DMEM and Ac-YVAD-cmk were included as the negative control. Spleen samples were collected on 5 days p.i. (dpi) and were either fixed and stained with antibodies against IL-1β and SFTSV NP (O) or were processed for IL-1β levels determination with ELISA analysis (P). Scale bars represent 50 μm.

Comparison of mean values (A, E, G, H, J–M, and P) between two groups was analyzed by Student's t test. Data shown are means ± SD. *$p < 0.05$; **$p < 0.01$; ***$p < 0.001$; ****$p < 0.0001$; ns, no significance. See also Figure S11.

was observed. It is tempting to speculate that the SFTSV-induced upregulation of BAK facilitates BAK/BAX activation, which results in mitochondrial inner membrane herniation into the cytosol. After being exposed into the cytosol, the compromised mitochondrial inner membrane, due to the downregulation of mitochondrial inner membrane proteins, allowed release of mtDNA into the cytosol, which triggers NLRP3 inflammasome activation. The mechanism of SFTSV-induced mitochondrial inner membrane protein downregulation and whether BAK can be employed as a biomarker for predicting SFTS disease progression would be interesting questions for further investigation.

The downstream event of BAK/BAX activation is the release of cytochrome *c* into the cytosol, which was observed in SFTSV-infected cells. Cytosolic cytochrome *c* drives the assembly of the so-called apoptosome, which leads to activation of caspase-9 and executioner caspase-3, resulting in cell apoptosis (Galluzzi and Vanpouille-Box, 2018). However, SFTSV infection did not induce strong apoptosis as indicated by Cell Counting Kit-8 (CCK-8) and lactate dehydrogenase (LDH) assay (Figures S11K and S11L). Our proteomic analysis revealed that several proteins with reported anti-apoptosis functions, such as SOD2, BCL3, CD74, FAM129B, etc., were upregulated during SFTSV infection, indicating a certain anti-apoptosis effect induced by the virus infection. It can be speculated that, in the absence of cell apoptosis, SFTSV-infected cells can induce enduring inflammatory responses leading to the SFTS-associated immunopathology.

Severe liver damage is a common symptom in SFTS patients, especially in fatal cases, and it was proposed that liver damage may play a central role in the pathogenesis of SFTSV infection (Hiraki et al., 2014; Liu et al., 2014; Sun et al., 2015). Inflammation is a major contributor to the pathogenesis of most acute and chronic liver damage (Szabo and Petrasek, 2015). Inflammatory responses mediated by liver macrophages, known as Kupffer cells, are reported to be the critical factor of inflammation-associated liver damage during HCV infection (Negash et al., 2013). SFTSV can productively infect macrophages inducing pronounced NLRP3 inflammatory responses. Additionally, other types of liver cells, including liver epithelial cells, are susceptible for SFTSV infection (Sun et al., 2015). It is possible that SFTSV infection of both hepatic cells and intrahepatic macrophages may synergistically result in strong liver damage, resulting in disease progression and eventually fatal outcome.

This study demonstrates that virus infection can trigger mtDNA release into the cytosol to activate the NLRP3 inflammatory responses. Considering the proposed mechanism that multiple stimuli trigger NLRP3 inflammasome activation through inducing cytosolic mtDNA release, it would be interesting to investigate whether other viruses, particularly those viruses that are known to cause severe inflammation-associated immune pathology such as influenza virus, also induce mtDNA release to trigger disease-associated NLRP3 inflammatory responses. Also, whether BAK/BAX activation-mediated mtDNA release is a common mechanism during virus infection could be investigated for other viruses. Such investigation should help to develop anti-inflammation strategies targeting the mechanism of mtDNA release to counteract severe immunopathology induced by a highly pathogenic virus.

STAR★METHODS

Detailed methods are provided in the online version of this paper and include the following:

- KEY RESOURCES TABLE
- LEAD CONTACT AND MATERIALS AVAILABILITY
- EXPERIMENTAL MODEL AND SUBJECT DETAILS
  - Cell lines
  - Human primary cells
  - Patients and samples
  - Mice
  - Viruses
- METHOD DETAILS
  - Cell differentiation
  - RNA isolation, cDNA library preparation and sequencing
  - Data analysis of RNA-seq
  - Quantitative proteomic analysis
  - Gene ontology (GO) analysis
  - Knockdown and knockout
  - RNA isolation and quantitative RT-PCR
  - Western blot analysis
  - Measurement of cytokine level
  - Measurements of caspase-1 activity
  - ASC oligomerization detection
  - Total and cytosolic DNA extraction
  - Quantification of mtDNA
  - Immunoprecipitation
  - EdU click-labeling and immunofluorescence Microscopy
  - Cell viability and Cytotoxicity assay
  - Measurement of mitochondrial membrane potential and ROS
  - Mitochondrial DNA depletion
  - Detection of cytochrome *c* release
  - BAK overexpression
  - Animal study
- QUANTIFICATION AND STATISTICAL ANALYSIS
- DATA AND CODE AVAILABILITY

SUPPLEMENTAL INFORMATION

Supplemental Information can be found online at https://doi.org/10.1016/j.celrep.2020.02.105.

ACKNOWLEDGMENTS

This work was supported by the National Science and Technology Major Project (grant 2018ZX10101004001005), the National Key R&D Program of China (grants 2018YFA0507201, 2016YFC1200400, and 2016YFC1201905), the National Natural Science Foundation of China (grants 81825019, 81722041, 31770188, 81472005, 81473023, 31500144, and 31900144), and the Strategic Priority Research Program of the Chinese Academy of Sciences (grant XDB29010204). We would like to thank Dr. Ding Gao, Anna Du, Juan Min, Pei Zhang, and Bichao Xu from the Center for Instrumental Analysis and

Metrology, Wuhan Institute of Virology, Chinese Academy of Science for technical assistance.

AUTHOR CONTRIBUTIONS

K.P., L.-K.Z., and W.L. conceived and supervised the study. K.P., L.-K.Z., W.L., S.L., and H.L. participated in the study design, analyzed the data, and wrote the manuscript. S.L., H.L., Y.-L.Z., Q.-L.X., Z.-Q.G., X.C., X.-A.Z., X.-K.L., and K.P. performed the experiments. G.-F.X., P.-Y.L., and J.C. provided helpful discussion and comment on study results. All authors read and approved the manuscript.

DECLARATION OF INTERESTS

The authors declare no competing interests.

Received: June 24, 2019
Revised: December 18, 2019
Accepted: February 13, 2020
Published: March 31, 2020

REFERENCES

Aguirre, S., Luthra, P., Sanchez-Aparicio, M.T., Maestre, A.M., Patel, J., Lamothe, F., Fredericks, A.C., Tripathi, S., Zhu, T., Pintado-Silva, J., et al. (2017). Dengue virus NS2B protein targets cGAS for degradation and prevents mitochondrial DNA sensing during infection. Nat. Microbiol. *2*, 17037.

Amezquita, R.A., Lun, A.T.L., Becht, E., Carey, V.J., Carpp, L.N., Geistlinger, L., Marini, F., Rue-Albrecht, K., Risso, D., Soneson, C., et al. (2020). Orchestrating single-cell analysis with Bioconductor. Nat. Methods *17*, 137–145.

Chen, I.Y., and Ichinohe, T. (2015). Response of host inflammasomes to viral infection. Trends Microbiol. *23*, 55–63.

Chung, I.C., Yuan, S.N., OuYang, C.N., Lin, H.C., Huang, K.Y., Chen, Y.J., Chung, A.K., Chu, C.L., Ojcius, D.M., Chang, Y.S., and Chen, L.C. (2018). Src-family kinase-Cbl axis negatively regulates NLRP3 inflammasome activation. Cell Death Dis. *9*, 1109.

Culshaw, A., Mongkolsapaya, J., and Screaton, G.R. (2017). The immunopathology of dengue and Zika virus infections. Curr. Opin. Immunol. *48*, 1–6.

Dang, E.V., McDonald, J.G., Russell, D.W., and Cyster, J.G. (2017). Oxysterol Restraint of Cholesterol Synthesis Prevents AIM2 Inflammasome Activation. Cell *171*, 1057–1071.e1011.

Dhir, A., Dhir, S., Borowski, L.S., Jimenez, L., Teitell, M., Rötig, A., Crow, Y.J., Rice, G.I., Duffy, D., Tamby, C., et al. (2018). Mitochondrial double-stranded RNA triggers antiviral signalling in humans. Nature *560*, 238–242.

Galluzzi, L., and Vanpouille-Box, C. (2018). BAX and BAK at the Gates of Innate Immunity. Trends Cell Biol. *28*, 343–345.

Gdula, M.R., Nesterova, T.B., Pintacuda, G., Godwin, J., Zhan, Y., Ozadam, H., McClellan, M., Moralli, D., Krueger, F., Green, C.M., et al. (2019). The non-canonical SMC protein SmcHD1 antagonises TAD formation and compartmentalisation on the inactive X chromosome. Nat. Commun. *10*, 30.

Gross, O., Thomas, C.J., Guarda, G., and Tschopp, J. (2011). The inflammasome: an integrated view. Immunol. Rev. *243*, 136–151.

He, Y., Hara, H., and Núñez, G. (2016). Mechanism and Regulation of NLRP3 Inflammasome Activation. Trends Biochem. Sci. *41*, 1012–1021.

He, Z., Chen, J., Zhu, X., An, S., Dong, X., Yu, J., Zhang, S., Wu, Y., Li, G., Zhang, Y., et al. (2018). NLRP3 Inflammasome Activation Mediates Zika Virus-Associated Inflammation. J. Infect. Dis. *217*, 1942–1951.

Hiraki, T., Yoshimitsu, M., Suzuki, T., Goto, Y., Higashi, M., Yokoyama, S., Tabuchi, T., Futatsuki, T., Nakamura, K., Hasegawa, H., et al. (2014). Two autopsy cases of severe fever with thrombocytopenia syndrome (SFTS) in Japan: a pathognomonic histological feature and unique complication of SFTS. Pathol. Int. *64*, 569–575.

Huang da, W., Sherman, B.T., and Lempicki, R.A. (2009). Systematic and integrative analysis of large gene lists using DAVID bioinformatics resources. Nat. Protoc. *4*, 44–57.

Kanneganti, T.D., Kundu, M., and Green, D.R. (2015). Innate immune recognition of mtDNA—an undercover signal? Cell Metab. *21*, 793–794.

Kim, K.H., Yi, J., Kim, G., Choi, S.J., Jun, K.I., Kim, N.H., Choe, P.G., Kim, N.J., Lee, J.K., and Oh, M.D. (2013). Severe fever with thrombocytopenia syndrome, South Korea, 2012. Emerg. Infect. Dis. *19*, 1892–1894.

Kim, D., Paggi, J.M., Park, C., Bennett, C., and Salzberg, S.L. (2019). Graph-based genome alignment and genotyping with HISAT2 and HISAT-genotype. Nat. Biotechnol. *37*, 907–915.

Krasich, R., and Copeland, W.C. (2017). DNA polymerases in the mitochondria: A critical review of the evidence. Front. Biosci. *22*, 692–709.

Lai, J.H., Wang, M.Y., Huang, C.Y., Wu, C.H., Hung, L.F., Yang, C.Y., Ke, P.Y., Luo, S.F., Liu, S.J., and Ho, L.J. (2018). Infection with the dengue RNA virus activates TLR9 signaling in human dendritic cells. EMBO Rep. *19*, e46182.

Lamkanfi, M., and Dixit, V.M. (2014). Mechanisms and functions of inflammasomes. Cell *157*, 1013–1022.

Latz, E., Xiao, T.S., and Stutz, A. (2013). Activation and regulation of the inflammasomes. Nat. Rev. Immunol. *13*, 397–411.

Lazear, H.M., Govero, J., Smith, A.M., Platt, D.J., Fernandez, E., Miner, J.J., and Diamond, M.S. (2016). A Mouse Model of Zika Virus Pathogenesis. Cell Host Microbe *19*, 720–730.

Li, H., Lu, Q.B., Xing, B., Zhang, S.F., Liu, K., Du, J., Li, X.K., Cui, N., Yang, Z.D., Wang, L.Y., et al. (2018). Epidemiological and clinical features of laboratory-diagnosed severe fever with thrombocytopenia syndrome in China, 2011-17: a prospective observational study. Lancet Infect. Dis. *18*, 1127–1137.

Liu, Y., Wu, B., Paessler, S., Walker, D.H., Tesh, R.B., and Yu, X.J. (2014). The pathogenesis of severe fever with thrombocytopenia syndrome virus infection in alpha/beta interferon knockout mice: insights into the pathologic mechanisms of a new viral hemorrhagic fever. J. Virol. *88*, 1781–1786.

Liu, J., Xu, M., Tang, B., Hu, L., Deng, F., Wang, H., Pang, D.W., Hu, Z., Wang, M., and Zhou, Y. (2019). Single-Particle Tracking Reveals the Sequential Entry Process of the Bunyavirus Severe Fever with Thrombocytopenia Syndrome Virus. Small *15*, e1803788.

Luo, L.M., Zhao, L., Wen, H.L., Zhang, Z.T., Liu, J.W., Fang, L.Z., Xue, Z.F., Ma, D.Q., Zhang, X.S., Ding, S.J., et al. (2015). Haemaphysalis longicornis Ticks as Reservoir and Vector of Severe Fever with Thrombocytopenia Syndrome Virus in China. Emerg. Infect. Dis. *21*, 1770–1776.

Majer, O., Liu, B., and Barton, G.M. (2017). Nucleic acid-sensing TLRs: trafficking and regulation. Curr. Opin. Immunol. *44*, 26–33.

Man, S.M., and Kanneganti, T.D. (2015). Regulation of inflammasome activation. Immunol. Rev. *265*, 6–21.

McArthur, K., Whitehead, L.W., Heddleston, J.M., Li, L., Padman, B.S., Oorschot, V., Geoghegan, N.D., Chappaz, S., Davidson, S., San Chin, H., et al. (2018). BAK/BAX macropores facilitate mitochondrial herniation and mtDNA efflux during apoptosis. Science *359*, eaao6047.

Mendoza-Parra, M.A., Van Gool, W., Mohamed Saleem, M.A., Ceschin, D.G., and Gronemeyer, H. (2013). A quality control system for profiles obtained by ChIP sequencing. Nucleic Acids Res. *41*, e196.

Mills, E.L., Kelly, B., and O'Neill, L.A.J. (2017). Mitochondria are the powerhouses of immunity. Nat. Immunol. *18*, 488–498.

Negash, A.A., Ramos, H.J., Crochet, N., Lau, D.T., Doehle, B., Papic, N., Delker, D.A., Jo, J., Bertoletti, A., Hagedorn, C.H., and Gale, M., Jr. (2013). IL-1β production through the NLRP3 inflammasome by hepatic macrophages links hepatitis C virus infection with liver inflammation and disease. PLoS Pathog. *9*, e1003330.

Paules, C.I., Marston, H.D., Bloom, M.E., and Fauci, A.S. (2018). Tickborne Diseases - Confronting a Growing Threat. N. Engl. J. Med. *379*, 701–703.

Pertea, M., Pertea, G.M., Antonescu, C.M., Chang, T.C., Mendell, J.T., and Salzberg, S.L. (2015). StringTie enables improved reconstruction of a transcriptome from RNA-seq reads. Nat. Biotechnol. *33*, 290–295.

Place, D.E., and Kanneganti, T.D. (2018). Recent advances in inflammasome biology. Curr. Opin. Immunol. *50*, 32–38.

Rainey, T., Occi, J.L., Robbins, R.G., and Egizi, A. (2018). Discovery of Haemaphysalis longicornis (Ixodida: Ixodidae) Parasitizing a Sheep in New Jersey, United States. J. Med. Entomol. *55*, 757–759.

Riley, J.S., Quarato, G., Cloix, C., Lopez, J., O'Prey, J., Pearson, M., Chapman, J., Sesaki, H., Carlin, L.M., Passos, J.F., et al. (2018). Mitochondrial inner membrane permeabilisation enables mtDNA release during apoptosis. EMBO J. *37*, e99238.

Rongvaux, A., Jackson, R., Harman, C.C., Li, T., West, A.P., de Zoete, M.R., Wu, Y., Yordy, B., Lakhani, S.A., Kuan, C.Y., et al. (2014). Apoptotic caspases prevent the induction of type I interferons by mitochondrial DNA. Cell *159*, 1563–1577.

Salic, A., and Mitchison, T.J. (2008). A chemical method for fast and sensitive detection of DNA synthesis in vivo. Proc. Natl. Acad. Sci. USA *105*, 2415–2420.

Shadel, G.S., and Horvath, T.L. (2015). Mitochondrial ROS signaling in organismal homeostasis. Cell *163*, 560–569.

Shimada, K., Crother, T.R., Karlin, J., Dagvadorj, J., Chiba, N., Chen, S., Ramanujan, V.K., Wolf, A.J., Vergnes, L., Ojcius, D.M., et al. (2012). Oxidized mitochondrial DNA activates the NLRP3 inflammasome during apoptosis. Immunity *36*, 401–414.

Shin, E.C., Sung, P.S., and Park, S.H. (2016). Immune responses and immunopathology in acute and chronic viral hepatitis. Nat. Rev. Immunol. *16*, 509–523.

Soutar, M.P.M., Kempthorne, L., Annuario, E., Luft, C., Wray, S., Ketteler, R., Ludtmann, M.H.R., and Plun-Favreau, H. (2019). FBS/BSA media concentration determines CCCP's ability to depolarize mitochondria and activate PINK1-PRKN mitophagy. Autophagy *15*, 2002–2011.

Sun, Q., Jin, C., Zhu, L., Liang, M., Li, C., Cardona, C.J., Li, D., and Xing, Z. (2015). Host Responses and Regulation by NFκB Signaling in the Liver and Liver Epithelial Cells Infected with A Novel Tick-borne Bunyavirus. Sci. Rep. *5*, 11816.

Szabo, G., and Petrasek, J. (2015). Inflammasome activation and function in liver disease. Nat. Rev. Gastroenterol. Hepatol. *12*, 387–400.

Takahashi, T., Maeda, K., Suzuki, T., Ishido, A., Shigeoka, T., Tominaga, T., Kamei, T., Honda, M., Ninomiya, D., Sakai, T., et al. (2014). The first identification and retrospective study of Severe Fever with Thrombocytopenia Syndrome in Japan. J. Infect. Dis. *209*, 816–827.

Tran, X.C., Yun, Y., Van An, L., Kim, S.H., Thao, N.T.P., Man, P.K.C., Yoo, J.R., Heo, S.T., Cho, N.H., and Lee, K.H. (2019). Endemic Severe Fever with Thrombocytopenia Syndrome, Vietnam. Emerg. Infect. Dis. *25*, 1029–1031.

van der Maaten, L., and Hinton, G. (2008). Visualizing Data Using t-SNE. J. Mach. Learn. Res. *9*, 2579–2605.

Wang, W., Li, G., De Wu, Luo, Z., Pan, P., Tian, M., Wang, Y., Xiao, F., Li, A., Wu, K., et al. (2018). Zika virus infection induces host inflammatory responses by facilitating NLRP3 inflammasome assembly and interleukin-1β secretion. Nat. Commun. *9*, 106.

West, A.P., and Shadel, G.S. (2017). Mitochondrial DNA in innate immune responses and inflammatory pathology. Nat. Rev. Immunol. *17*, 363–375.

West, A.P., Khoury-Hanold, W., Staron, M., Tal, M.C., Pineda, C.M., Lang, S.M., Bestwick, M., Duguay, B.A., Raimundo, N., MacDuff, D.A., et al. (2015). Mitochondrial DNA stress primes the antiviral innate immune response. Nature *520*, 553–557.

Yamada, S., Shimojima, M., Narita, R., Tsukamoto, Y., Kato, H., Saijo, M., and Fujita, T. (2018). RIG-I-Like Receptor and Toll-Like Receptor Signaling Pathways Cause Aberrant Production of Inflammatory Cytokines/Chemokines in a Severe Fever with Thrombocytopenia Syndrome Virus Infection Mouse Model. J. Virol. *92*, e02246-17.

Yu, X.J., Liang, M.F., Zhang, S.Y., Liu, Y., Li, J.D., Sun, Y.L., Zhang, L., Zhang, Q.F., Popov, V.L., Li, C., et al. (2011). Fever with thrombocytopenia associated with a novel bunyavirus in China. N. Engl. J. Med. *364*, 1523–1532.

Zhong, Z., Liang, S., Sanchez-Lopez, E., He, F., Shalapour, S., Lin, X.J., Wong, J., Ding, S., Seki, E., Schnabl, B., et al. (2018). New mitochondrial DNA synthesis enables NLRP3 inflammasome activation. Nature *560*, 198–203.

Zhou, R., Yazdi, A.S., Menu, P., and Tschopp, J. (2011). A role for mitochondria in NLRP3 inflammasome activation. Nature *469*, 221–225.

Zhuang, L., Sun, Y., Cui, X.M., Tang, F., Hu, J.G., Wang, L.Y., Cui, N., Yang, Z.D., Huang, D.D., Zhang, X.A., et al. (2018). Transmission of Severe Fever with Thrombocytopenia Syndrome Virus by Haemaphysalis longicornis Ticks, China. Emerg. Infect. Dis. *24*, 868–871.

STAR★METHODS

KEY RESOURCES TABLE

REAGENT or RESOURCE	SOURCE	IDENTIFIER
Antibodies		
Rabbit monoclonal anti-NLRP3 (D2P5E)	Cell Signaling Technology	Cat# 13158; RRID:AB_2798134
Rabbit monoclonal anti-MyD88 (D80F5)	Cell Signaling Technology	Cat# 4283; RRID:AB_10547882
Rabbit monoclonal anti-MAVS (D5A9E)	Cell Signaling Technology	Cat# 24930; RRID:AB_2798889
Rabbit polyclonal anti-caspase-1	Cell Signaling Technology	Cat# 2225; RRID:AB_2243894
Rabbit polyclonal anti-IL-1β	ABclonal	Cat# A1112; RRID:AB_2758416
Rabbit polyclonal anti-BAK1	ABclonal	Cat# A0498; RRID:AB_2757224
Rabbit polyclonal anti-BAX	ABclonal	Cat# A15646; RRID:AB_2763052
Rabbit polyclonal anti-IL1RN	ABclonal	Cat# A2088; RRID:AB_2764108
Rabbit polyclonal anti-NNT	ABclonal	Cat# A4561; RRID:AB_2765755
Rabbit polyclonal anti-IMMT	ABclonal	Cat# A2751; RRID:AB_2764600
Rabbit polyclonal anti-COX5A	ABclonal	Cat# A6437; RRID:AB_2767039
Mouse monoclonal anti-Cytochrome *c* (2D8D11)	Proteintech	Cat# 66264-1-Ig; RRID:AB_2716798
Rabbit polyclonal anti-α-Tubulin	Proteintech	Cat# 14555-1-AP; RRID:AB_2212258
Rabbit polyclonal anti-MX1	Proteintech	Cat# 13750-1-AP; RRID:AB_2266768
Rabbit polyclonal anti-PML	Proteintech	Cat# 21041-1-AP
Mouse monoclonal anti-ASC	Santa Cruz Biotechnology	Cat# sc-271054; RRID:AB_10608960
Mouse monoclonal anti-TOM20	Santa Cruz Biotechnology	Cat# sc-17764; RRID:AB_628381
Mouse monoclonal anti-8-OH-dG	Santa Cruz Biotechnology	Cat# sc-66036; RRID:AB_832272
Mouse monoclonal anti-Lamin A/C	Santa Cruz Biotechnology	Cat# sc-376248; RRID:AB_10991536
Mouse monoclonal anti-BrdU	Sigma-Aldrich	Cat# B8434; RRID:AB_476811
Rabbit polyclonal anti-IL-1β	Abcam	Cat# ab9722; RRID:AB_308765
Rabbit polyclonal anti-Calnexin	Abcam	Cat# ab22595; RRID:AB_2069006
Rabbit polyclonal anti-SAMD9	ABMART	Cat# X-C9JKF1
Rabbit polyclonal anti-NP	This paper	N/A
Bacterial and Virus Strains		
SFTSV isolate HBMC16, GenBank: KY440775.1, KY440776.1 and KY440777.1	Isolated from patient	N/A
Biological Samples		
Peripheral blood from healthy and SFTSV infected adults	This paper	N/A
Chemicals, Peptides, and Recombinant Proteins		
Lipopolysaccharide (LPS)	Sigma-Aldrich	Cat# L4391
Phorbol-12-myristate-13-acetate (PMA)	Sigma-Aldrich	Cat# P1585
Disuccinimidyl suberate (DSS)	Sigma-Aldrich	Cat# S1885
Digitonin	Sigma-Aldrich	Cat# D141
Carbonyl cyanide 3-chlorophenylhydrazone (CCCP)	Sigma-Aldrich	Cat# C2759
Nigericin	InvivoGene Biotech	Cat# tlrl-nig
Ac-YVAD-cmk	InvivoGene Biotech	Cat# inh-yvad
VX-765	Selleck	Cat# S222
MCC950	Selleck	Cat# S7809
MLN120B	MedChemExpress	Cat# HY-15473
Staurosporine (STS)	MedChemExpress	Cat# HY-15141
Deoxyguanosine (dG)	MedChemExpress	Cat# HY-17563
Ficoll-Paque plus	GE Healthcare	Cat# 17144002

(*Continued on next page*)

Continued

REAGENT or RESOURCE	SOURCE	IDENTIFIER
Ethidium Bromide (EtBr)	Sangon	Cat# A500328
Mito-TEMPO	Santa Cruz Biotechnology	Cat# sc-221945
8-OH-dG	Ruibio	Cat# TH3846
Trizol	Thermo Fisher	*Cat# 15596018*
Lipofectamine 2000	Thermo fisher	*Cat# 11668019*
Mito-SOX	Thermo Fisher	Cat# M36008
Tetramethyl rhodamine methyl ester (TMRM)	Thermo Fisher	Cat# T668
Critical Commercial Assays		
EasySepTM Human Monocyte Isolation Kit	STEMCELL Technologies	Cat# 19359
EasySepTM Direct Human Total Lymphocyte Isolation Kit	STEMCELL Technologies	Cat# 19655
NEB Next Ultra RNA Library Prep Kit	New England Biolabs	Cat# E7335
NEB Next Poly (A) mRNA Magnetic Isolation Module kit	New England Biolabs	Cat# E7490
KAPA Library Quantification kit	KAPA Biosystems	Cat# KK4824
iTRAQ reagents	SCIEX	Cat# 4352135
FastPure Cell/Tissue Total RNA Isolation Mini Kit	Vazyme	Cat# RC101-01
HiScript II One Step qRT-PCR SYBR Green Kit	Vazyme	Cat# Q221-01
Immobilon ECL Ultra Western HRP Substrate	Millipore	Cat# WBULS0500
Human IL-1β ELISA Set II	BD Biosciences	Cat# 557953
Caspase 1 Activity Assay Kit	Beyotime	Cat# C1102
DNeasy Blood &Tissue Kit	QIAGEN	Cat# 69506
TB Green® Premix Ex Taq II	Takara	Cat# RR820A
Pierce Classic Magnetic IP/Co-IP Kit	Thermo Fisher Scientific	Cat# 88804
Click-iT EdU-Alexa Fluor 647 Imaging Kit	Life Technologies	Cat# C10340
Cell Counting kit-8 (CCK-8)	Dojindo Molecular Technologies	Cat# CK04
LDH Cytotoxicity Assay Kit	Beyotime	Cat# C0016
Mouse IL-1β ELISA Kit	Abcam	Cat# ab197742
Deposited Data		
RNA-sequencing data	GEO	GSE144358
Proteomics data	ProteomeXchange	PXD017224
Experimental Models: Cell Lines		
Monkey: Vero cells	ATCC	Cat# CCL81
Human: THP-1 cells	ATCC	Cat# TIB-202
Human: HEK293T cells	ATCC	Cat# CRL-11268
Experimental Models: Organisms/Strains		
Mouse: C57BL/6	Charles River	N/A
Oligonucleotides		
Primer:BAK1 Forward: GAGGAATTCA TGGCTTCGGGGCAAGGC	This paper	N/A
Primer:BAK1 Reverse: CGCGGATCCTCAT GATTTGAAGAATCTTCGTACC	This paper	N/A
Software and Algorithms		
GraphPad Prism version 6	GraphPad Software	https://www.graphpad.com/
Snapgene Viewer	Snapgene	https://www.snapgene.com/
t-SNE	van der Maaten and Hinton, 2008	http://lvdmaaten.github.io/tsne/
DAVID v6.8	Huang da et al., 2009	https://david.ncifcrf.gov/
FastQC v0.11.5	Gdula et al., 2019	https://www.bioinformatics.babraham.ac.uk/projects/fastqc/
NGSQC v2.3.3	Mendoza-Parra et al., 2013	http://www.ngs-qc.org/

(*Continued on next page*)

Continued

REAGENT or RESOURCE	SOURCE	IDENTIFIER
HISAT2 v2.0.5	Kim et al., 2019	https://daehwankimlab.github.io/hisat2/
StringTie v1.3.3b	Pertea et al., 2015	https://ccb.jhu.edu/software/stringtie/
DESeq v1.28.0	Amezquita et al., 2020	http://bioconductor.org/packages/release/bioc/html/DESeq.html
ImageJ	NIH, Univ. of Wisc. Madison	https://imagej.nih.gov/ij/

LEAD CONTACT AND MATERIALS AVAILABILITY

Further information and requests for resources and reagents should be directed to and will be fulfilled by the Lead Contact, Dr. Ke Peng (pengke@wh.iov.cn).

All shRNAs and sgRNAs generated in this study are available from the Lead Contact without restriction.

EXPERIMENTAL MODEL AND SUBJECT DETAILS

Cell lines

Vero cells and HEK293T cells were obtained from American Type Culture Collection (ATCC) and maintained in Dulbecco's modified Eagle's medium (DMEM; GIBCO) supplemented with 10% fetal bovine serum (FBS; GIBCO) and 1% antibiotics (GIBCO) at 37°C in a humidified atmosphere of 5% CO_2. THP-1 cells were obtained from ATCC, and cultured in RPMI-1640 medium containing 10% FBS and antibiotics at 37°C in a humidified atmosphere of 5% CO_2.

Human primary cells

Heparinized peripheral blood was collected from healthy volunteers. Written informed consent was obtained from all subjects and the research was approved by the responsible ethics committee (Ethics committee of Wuhan Institute of Virology, Chinese Academy of Sciences). Peripheral blood mononuclear cells (PBMCs) were obtained by density gradient centrifugation using Ficoll-Paque plus (followed manufacturers' protocol). After isolation, PBMCs were cultured in RPMI 1640 medium (Thermo Fisher Scientific) supplemented with 10% heat inactivated FBS at 37°C. For preparation of monocyte-derived macrophages (MDMs), PBMCs were isolated as described above, and seeded in RPMI 1640 medium supplemented with 10% heat inactivated FBS overnight at 37°C. Non-adherent cells were removed and adherent monocytes were washed, followed by cultivation in RPMI 1640 containing 10% heat inactivated FBS and 10% human AB serum (Sigma Aldrich, St. Louis, USA) at 37°C for 7 days to differentiate into macrophages. Monocyte and lymphocyte were isolated with EasySepTM Human Monocyte Isolation Kit (19359, STEMCELL Technologies, Vancouver, Canada) and EasySepTM Direct Human Total Lymphocyte Isolation Kit (19655, STEMCELL Technologies, Vancouver, Canada) according to manufacturer's instructions.

Patients and samples

A case-control study was performed at the People's Liberation Army 154 hospital, the designated hospital for SFTS in Xinyang City, Henan Province, China, to identify differentially expressed genes in SFTSV infection. Adult patients who were admitted to the hospital from May to August 2016 and confirmed to be infected with SFTSV according to the guidelines released by China Ministry of Health were recruited in the current study. Patients with tumor, tuberculosis, diabetes, or other infections (i.e., hepatitis virus, dengue virus, *Rickettsia*, and *Borrelia*), were excluded. The research protocol was approved by the human ethics committee of the hospital in accordance with the medical research regulations of China, and all participants provided written informed consent to have their samples and information collected.

Data about demography, clinical features, laboratory data, and outcome, were retrospectively collected. For the patients who discontinued therapy or had been discharged from hospital because of adverse clinical progression, we made follow-up visits within two weeks of discharge by phone call or home visiting to determine their final outcome (death or survival). The recruited cases had their peripheral blood samples collected using the PAXgene Blood RNA tube (BD Biosciences) at the acute phase of illness when admitted to the hospital and at the convalescent phase when discharged from the hospital.

Mice

Five-week-old female C57BL/6 mice purchased from Charles River Laboratories (Beijing, China) were kept in an environmentally controlled specific-pathogen-free (SPF) animal facility in the Laboratory Animal Center of Academy of Military Medical Sciences (Beijing, China). Animal experiment was approved by the Institutional Animal Care and Use Committee and was performed in accordance with the National Institutes of Health guidelines under protocols.

Viruses

The SFTSV isolate HBMC16 (GenBank: KY440775.1, KY440776.1 and KY440777.1) isolated by Wuhan Institute of Virology, Chinese Academy of Sciences (Wuhan, Hubei, China) was propagated in Vero cells and used in this study. Viral titer was determined by focus-forming assay on Vero cells. Briefly, confluent monolayers were incubated with 10-fold dilutions of virus for 1 hour, then culture medium was replaced by DMEM containing 2% serum and supplemented with 1.1% carboxymethyl-cellulose. Foci were visualized by two-step immunostaining with an antibody against viral protein NP and an anti-rabbit horseradish peroxidase-conjugated secondary antibody (Proteintech). Virus was inactivated by exposing to ultraviolet (UV) light for 3 hours, and the inactivation was confirmed by focus-forming assay on Vero cells.

METHOD DETAILS

Cell differentiation

THP-1 cells were differentiated into macrophages by treatment with 40 ng/mL of PMA for 24 hours at 37°C, and cells were cultured without PMA for 24 hours.

RNA isolation, cDNA library preparation and sequencing

Whole blood cells were collected and total RNA was extracted with Trizol (Tiangen, Beijing) and assessed with Agilent 2100 BioAnalyzer (Agilent Technologies, Santa Clara, CA, USA) and Qubit Fluorometer (Invitrogen). Total RNA samples that meet the following requirements were used in subsequent experiments: RNA integrity number (RIN) > 7.0 and a 28S:18S ratio > 1.8.RNA-seq libraries were generated and sequenced by CapitalBio Technology (Beijing, China). The triplicate samples of all assays were constructed an independent library, and do the following sequencing and analysis. The NEB Next Ultra RNA Library Prep Kit for Illumina (NEB) was used to construct the libraries for sequencing. NEB Next Poly (A) mRNA Magnetic Isolation Module kit was used to enrich the poly (A) tailed mRNA molecules from 1 μg total RNA. The mRNA was fragmented into ~200 base pair pieces. The first-strand cDNA was synthesized from the mRNA fragments reverse transcriptase and random hexamer primers, and then the second-strand cDNA was synthesized using DNA polymerase I and RNaseH. The end of the cDNA fragment was subjected to an end repair process that included the addition of a single "A" base, followed by ligation of the adapters. Products were purified and enriched by polymerase chain reaction (PCR) to amplify the library DNA. The final libraries were quantified using KAPA Library Quantification kit (KAPA Biosystems, South Africa) and an Agilent 2100 Bioanalyzer. After quantitative reverse transcription-PCR validation, libraries were subjected to paired-end sequencing with pair end 150-base pair reading length on an Illumina HiSeq sequencer (Illumina).

Data analysis of RNA-seq

The genome of human genome version of hg19 was used as reference. The sequencing quality were assessed with FastQC (v0.11.5) (Gdula et al., 2019) and then low quality data were filtered using NGSQC (v2.3.3) (Mendoza-Parra et al., 2013).The clean reads were then aligned to the reference genome using HISAT2 (v2.0.5) (Kim et al., 2019) with default parameters. The processed reads from each sample were aligned using HISAT2 against the reference genome. The gene expression analyses were performed with StringTie (v1.3.3b) (Pertea et al., 2015). DESeq (v1.28.0) (Amezquita et al., 2020) was used to analyze the DEGs between samples. Thousands of independent statistical hypothesis testing was conducted on DEGs, separately. Then a p value was obtained, which was corrected by FDR method. And Corrected P value (q-value) was calculated by correcting using BH method. P value or q value were used to conduct significance analysis. Parameters for classifying significantly DEGs are e2-fold differences ($|\log2FC| \geq 1$, FC: the fold change of expressions) in the transcript abundance and $p < 0.05$.

Quantitative proteomic analysis

THP-1 cells were infected with SFTSV at an MOI of 1 or mock infected. At 24, 48, 72 hours p.i., cells were harvested and total proteins were extracted. Extracted proteins were reduced with DTT, alkylated with iodoacetomide, and digested with trypsin. The digested peptides were desalted with a SepPak C18 cartridge (Waters). For iTRAQ labeling, 100 μg of peptides from SFTSV- or mock-infected cells was labeled with different iTRAQ reagents (SCIEX) according to manufacturer's instructions, and then were mixed at the ratio of 1 and desalted. The mixed peptides were fractionated using strong cation exchange. Fractionated peptides were subjected to LC-MS/MS analysis on a quadrupole-time of flight LC/MS/MS mass spectrometer (TripleTOF 5600+, SCIEX) equipped with a nanospray source. For MS/MS analysis, each scan cycle consisted of one full-scan mass spectrum followed by 20 MS/MS events. Mass spectra were extracted by Peakview v2.0 (SCIEX).

Mass spectra were submitted to ProteinPilot v5.0.1 (SCIEX) to perform protein identification and quantification. Search parameters were as follows: Sample Type: iTRAQ 8plex (Peptide labeled); Cysteine Alkylation: Iodoacetamide; Digestion: Trypsin; Fixed modification: carbamidomethyl Cys; Variable modification: none; Instrument: TripleTOF 5600. The false discovery rate (FDR) was set as lower than 1% at the protein level, and only peptides with confidence score > 95% were used.

Protein ratio in each replicate was calculated from the weighted average ratios of its peptides. The protein ratio values used for bioinformatics analysis were the weighted averages of the six replicates (three independent biological replicates and two technical replicates in each independent biological replicate), while the p value for protein ratio was calculated and further corrected with multiple Bonferroni correction. The Gaussian distribution of protein ratios was analyzed, and value deviating from the mean of the

normally distributed data by 1.96 standard deviations was considered as cutoff value. Only proteins with 1) ratios > upregulated or < downregulated cutoff values; 2) corrected p value for protein ratio < 0.05 was considered as be differentially regulated.

Gene ontology (GO) analysis

To perform GO analysis, differentially regulated proteins were submitted to DAVID (Huang da et al., 2009) (https://david.ncifcrf.gov/). Proteins were classified into different categories, and a statistical over-representation test was performed. P values were assessed with a binomial test and corrected for multiple testing using a Bonferroni procedure. Only categories with a p value < 0.05 were considered as over- or under- represented.

Knockdown and knockout

Knockdown of MAVS, MyD88, TLR7, TLR8, NLRP3, ASC, Caspase1, POLG, BAK or BAX was done by lentiviral transduction of THP-1 cells. Knockout of TLR7 was accomplished by transduction of THP-1 cells with lentiviruses expressing Cas9 and specific sgRNAs targeting TLR7. Sequences of targeting shRNAs (from Sigma shRNA Mission library) and sgRNAs used in this study are available upon request.

RNA isolation and quantitative RT-PCR

Total RNA was extracted with FastPure Cell/Tissue Total RNA Isolation Mini Kit (Vazyme, China) following the manufacturer's instructions. Quantitative RT-PCR was performed using the HiScript II One Step qRT-PCR SYBR Green Kit (Vazyme, China). Primer sequences are available upon request.

Western blot analysis

Cells treated as indicated were lysed with buffer (50 mM Tris, pH 7.5, 150 mM NaCl, 1% NP40, 5 mM EDTA, and 10% glycerol). Cell lysates was subjected to 12%–15% SDS-polyacrylamide gel electrophoresis (PAGE) and then transferred to polyvinylidene difluoride (PVDF) membranes (Millipore). Proteins were further incubated with the indicated primary antibodies and then horseradish peroxidase-conjugated secondary antibodies. Protein bands were detected by an enhanced chemiluminescence (ECL) kit (Millipore) using a Chemiluminescence Analyzer (Chemiscope600pro).

Measurement of cytokine level

IL1β, IL6, IL10, and TNF-α levels in serum samples were measured by immunoassay with Luminex xMAP technology (Luminex, Austin, TX, USA). Tests were performed according to the manufacturer's recommendations and the results were recorded as pg/ml. Data were acquired using Luminex 200 system and these cytokine levels were quantified using a logistic regression curve derived from the reference standards supplied by the manufacturer. The concentrations of IL-1β in culture supernatants were measured by the ELISA Kit (BD Biosciences, San Jose, CA, USA) according to the manufacturer's protocol.

Measurements of caspase-1 activity

THP-1^{PMA} cells were treated with LPS and Nigericin or infected with SFTSV. Caspase-1 activity in lysates was detected by commercial assay kits (Caspase 1 Activity Assay Kit) according to the manufacturer's instructions. The infected cells were lysed and centrifuged at 16,000 × g for 15 min at 4°C. The supernatants were collected and incubated with Ac-YVAD-pNA for 2 hours at 37°C in dark. The absorbance values were measured by a microplate reader at a wavelength of 405 nm. The caspase-1 activity was calculated by the standard curve of pNA. The results are presented as relative activity of caspase-1 of the mock group.

ASC oligomerization detection

THP-1^{PMA} cells treated as indicated were lysed in ice-cold buffer containing 50 mM Tris, pH 7.5, 150 mM NaCl, 1% NP40, 5 mM EDTA, and 10% glycerol. The cell lysates were then centrifuged at 6000 × g for 15 min at 4°C, and the supernatants were mixed with SDS loading buffer for western blotting analyses using indicated antibodies. The pellets were washed and cross-linked with fresh DSS (4 mM) (Sigma-Aldrich, St. Louis, MO, USA) at 37°C for 30 min. The cross-linked samples were centrifuged and mixed with SDS loading buffer for western blotting analysis using an antibody against ASC.

Total and cytosolic DNA extraction

The total and cytosolic DNA extraction was performed as described previously (West et al., 2015). Cells treated as indicated were divided into two equal aliquots. One aliquot, serve as normalization control, was subjected to total DNA extraction using DNeasy Blood &Tissue Kit (QIAGEN, Germany). The other aliquot was re-suspended in digitonin fractionation buffer (150 mM NaCl, 50 mM HEPES pH 7.4, 25 μg/ml digitonin). The samples were rotated for 10 min at 4°C and then centrifuged at 980 × g for 3 min three times to remove cellular debris. The cytosolic supernatants were then transferred to fresh tubes and spun at 17,000 × g for 10 min to remove remaining cellular debris. The cytosolic DNA was then extracted by DNeasy Blood &Tissue Kit (QIAGEN, Germany).

Quantification of mtDNA

To quantify mtDNA level, extracted DNA was subjected to quantitative PCR with TB Green® *Premix Ex Taq* II (Takara, Japan). The levels of total mtDNA were calculated as mtDNA normalized to *nGAPDH*. To measure cytosolic mtDNA, 20 ng of a purified plasmid encoding *eGFP* gene was added to the eluted solution as described previously (Aguirre et al., 2017). The relative content of cytosolic mtDNA was normalized to *eGFP*. The relative content of cytosolic versus total mtDNA was calculated.

Immunoprecipitation

THP-1^{PMA} cells were preloaded with BrdU (10 μM, Sigma) for 48 hours and treated as indicated. The cells were collected and washed twice with PBS. Immunoprecipitation was performed using the Pierce Classic Magnetic IP/Co-IP Kit (Thermo Fisher Scientific) according to manufacturer's protocols. In brief, cells were lysed and incubated with rabbit anti-NLRP3 antibody (CST), rotated overnight at 4°C. Subsequently, magnetic beads were added and incubated with lysates on a rotator for 1 hour at RT. After washing, the associated fractions were eluted from the beads. For detection of BrdU and 8-OH-dG, eluted fractions were dot-blotted and UV cross-linked to a nitrocellulose membrane. Immunoblotting was performed using anti-BrdU monoclonal antibody (Sigma) or anti-8OH-dG monoclonal antibody (Santa Cruz). DNA precipitation was extracted and detected by quantitative RT-PCR. 20 ng of plasmid encoding *eGFP* gene was added to the eluted solution, and the relative content of mtDNA was normalized to *eGFP* as described above.

EdU click-labeling and immunofluorescence Microscopy

THP-1^{PMA} cells were preloaded with EdU (10 μM, Life Technologies) for 24 hours and mock treated or infected with SFTSV at an MOI of 10. At 24 hours post infection, cells were washed with PBS and fixed with 4% paraformaldehyde (PFA) at room temperature for 30 min. Cells were washed and permeabilized with 0.2% (vol/vol) Triton X-100, and subsequently Click-labeled for 30 min at RT in dark using the Click-iT EdU-Alexa Fluor 647 Imaging Kit (Life Technologies) according to the manufacturer's protocols, followed by immunostaining with rabbit anti-NLRP3 antibody (CST) for 1 hour at RT and Alexa Fluor 488 goat anti-rabbit IgG for 1 hour (Life Technologies). After washing, cells were incubated with 4,6-diamidino-2-phenylindole (DAPI) solution for 10 min, then washed and mounted for analysis using confocal microscope (Andor Dragonfly 202).

For the immunostaining of 8-OH-dG, THP-1^{PMA} cells were mock treated or infected with SFTSV (MOI = 10) for 24 hours. Cells were fixed and permeabilized as described above, and then blocked with PBS containing 3% BSA for 10 min. The cells were incubated with mouse anti- 8-OH-dG (Santa Cruz) for 1 hour at RT, followed by incubation with Fluor 561 goat anti-mouse IgG for 1 hour. Cells were washed and incubated with DAPI, and then analyzed using confocal microscope (Andor Dragonfly 202).

Cell viability and Cytotoxicity assay

THP-1^{PMA} cells were treated as indicated. Cell viability was detected by Cell Counting kit-8 (CCK-8; Dojindo Molecular Technologies, Japan). Cell death was measured by a lactate dehydrogenase (LDH) assay using LDH Cytotoxicity Assay Kit (Beyotime, China).

Measurement of mitochondrial membrane potential and ROS

THP-1^{PMA} cells were mock treated or infected with SFTSV (MOI = 10) and stained with the mitochondrial membrane potential dye TMRM (Invitrogen) or mitochondrial superoxide indicator MitoSOX (Invitrogen) according to the manufacturer's instructions. Cells were loaded with 200 nM of TMRM for 30 min or 5 μM of MitoSOX for 15 min at 37°C, and then washed three times with PBS. TMRM fluorescence was measured using a multimode microplate reader (Perkin Elmer). MitoSOX fluorescence was measured by an epifluorescence microscope (Olympus IX73).

Mitochondrial DNA depletion

THP-1^{PMA} cells pretreated with ethidium bromide (EtBr, 450 ng/ml) for 48 or 96 hours were infected with SFTSV (MOI = 10). At 48 hours p.i., THP-1^{PMA} cells were collected and mitochondrial DNA depletion was assessed by total and cytosolic DNA extraction followed by quantitative PCR for mtDNA as described above.

Detection of cytochrome *c* release

Mock treated or SFTSV infected THP-1^{PMA} cells were subjected to digitonin fractionation as described previously and whole cell extracts (WCE), the first pellet after digitonin fractionation (Pel), or cytosolic extracts (Cyt) were blotted using antibody against cytochrome *c*.

BAK overexpression

The cDNAs of human BAK was obtained by reverse transcription of total RNA isolated from THP-1 cells, followed by PCR using gene specific primers (Forward: 5′-GAGGAATTCATGGCTTCGGGGCAAGGC-3′, Reverse: 5′-CGCGGATCCTCATGATTTGAAG AATCTTCGTACC-3′). The cDNAs was cloned into pCDH vector to construct plasmid expressing BAK, named pCDH-BAK. The pCDH vector or pCDH-BAK was transfected into HEK293T cells with Lipofectamine 2000 (11668019, Thermo fisher, USA).

Animal study

Five-week-old female C57BL/6 mice were divided into three groups: SFTSV + vehicle (1% Dimethyl sulfoxide solution in PBS) group (n = 7), SFTSV + Ac-YVAD-cmk group (n = 8), and DMEM + Ac-YVAD-cmk group (n = 5). For SFTSV infection, mice were treated with anti-IFNAR1 IgG (1.7 mg) by intraperitoneal injection at 1 day prior to infection. Mice were intraperitoneally inoculated with 10^3 FFU of SFTSV in 100 μL of DMEM at day 0, or the same volume of DMEM. Ac-YVAD-cmk (InvivoGen, USA) was dissolved in 1% Dimethyl sulfoxide solution and given by intraperitoneal injection with the dose of 8 mg/kg/d 1 h after SFTSV inoculation. Ac-YVAD-cmk was administered on a daily basis for 5 days and mice were monitored for 12 days. Animal experiment was approved by the Institutional Animal Care and Use Committee and was performed in accordance with the National Institutes of Health guidelines under protocols.

For the determination of IL-1β in spleen, mice were treated and infected as described above, mice from SFTSV group (n = 3), from SFTSV + Ac-YVAD-cmk group (n = 4) and from DMEM + Ac-YVAD-cmk group (n = 3) were sacrificed on 5 dpi. Spleen samples were collected after sacrifice. Concentrations of IL-1β in spleen were determined with the mouse IL-1β ELISA Kit (Abcam, Cambridge, UK) according to the manufacturer's instructions. Spleen samples were fixed in 4% formaldehyde in PBS at room temperature. The fixed tissues were paraffin-embedded, sectioned and processed for immunohistochemistry (IHC) using antibodies against mouse IL-1β (Abcam, Cambridge, UK) and SFTSV NP protein.

QUANTIFICATION AND STATISTICAL ANALYSIS

All statistical analyses were performed in GraphPad Prism version 6, as defined in the text and figure legends.

DATA AND CODE AVAILABILITY

RNA-Seq datasets are available at the NCBI under the accession number GEO: GSE144358. Proteomics datasets are available at the ProteomeXchange under the accession number: PXD017224.